PHYSICAL REVIEW B **82**, 174440 (2010)

Exotic phases induced by strong spin-orbit coupling in ordered double perovskites

Gang Chen
Physics Department, University of Colorado, Boulder, Colorado 80309, USA
and Physics Department, University of California, Santa Barbara, California 93106, USA

Rodrigo Pereira
Instituto de Fítsica de São Carlos, Universidade de São Paulo, CP 369, São Carlos 13566-970, SP, Brazil
and Kavli Institute for Theoretical Physics, University of California, Santa Barbara, California 93106, USA

Leon Balents
Kavli Institute for Theoretical Physics, University of California, Santa Barbara, California 93106, USA
(Received 26 September 2010; published 29 November 2010)

We construct and analyze a microscopic model for insulating rocksalt ordered double perovskites, with the chemical formula $A_2BB'O_6$, where the B' atom has a $4d^1$ or $5d^1$ electronic configuration and forms a face-centered-cubic lattice. The combination of the triply degenerate t_{2g} orbital and strong spin-orbit coupling forms local quadruplets with an effective spin moment $j=3/2$. Moreover, due to strongly orbital-dependent exchange, the effective spins have substantial biquadratic and bicubic interactions (fourth and sixth order in the spins, respectively). This leads, at the mean-field level, to three main phases: an unusual antiferromagnet with dominant octupolar order, a ferromagnetic phase with magnetization along the [110] direction, and a nonmagnetic but quadrupolar ordered phase, which is stabilized by thermal fluctuations and intermediate temperatures. All these phases have a two-sublattice structure described by the ordering wave vector $\boldsymbol{Q}=2\pi(001)$. We consider quantum fluctuations and argue that in the regime of dominant antiferromagnetic exchange, a nonmagnetic valence-bond solid or quantum-spin-liquid state may be favored instead. Candidate quantum-spin-liquid states and their basic properties are described. We also address the effect of single-site anisotropy driven by lattice distortions. Existing and possible future experiments are discussed in light of these results.

DOI: 10.1103/PhysRevB.82.174440 PACS number(s): 71.70.Ej, 71.70.Gm, 75.10.−b

I. INTRODUCTION

In magnetic Mott insulators with quenched orbital degrees of freedom, weak spin-orbit coupling (SOC) only leads to a small correction to the usual spin-exchange Hamiltonian in the form of single-site anisotropy and Dzyaloshinskii-Moriya interactions.[1,2] In the presence of strong SOC, however, a completely different physical picture emerges, in which spin itself is not a good quantum number, and magnetic anisotropy is usually large. Generally, strong SOC is common in the lanthanides, in which the relevant $4f$ electrons are very tightly bound to the nucleus. The tight-binding shields the electrons from crystal fields, which tend to split the orbital degeneracies involved in SOC, and moreover reduces exchange, which also competes with SOC.

While more rare, strong SOC is becoming an increasing focus in d-electron systems, in which electrons are more delocalized than in the lanthanides, and more diverse phenomena can be expected. For instance, strong SOC can be expected in $5d$ transition-metal compounds, which have large intrinsic atomic SOC due to their high atomic weight. In this category, many Ir-based magnets have been studied recently.[3,4] Lighter transition metals may also exhibit strong SOC if competing effects such as crystal fields and exchange are suppressed, e.g., by choosing crystal structures with high-symmetry and well-separated magnetic ions, respectively. An example of this type is the "spin-orbital liquid" state observed in the Fe-based spinel $FeSc_2S_4$,[5–7] which is believed to be driven by SOC.[8–10]

In this paper, we consider the case of insulating magnetic ordered double perovskites. Structurally, ordered double perovskites (with the chemical formula $A_2BB'O_6$) are derived from the usual perovskites ABO_3 by selectively replacing half the B ions with another species, denoted B'. We focus on the case in which the B ions are nonmagnetic and the B' ones are magnetic. Because of the difference in the valence charges and ionic radius between B and B' ions, the magnetic B' ions form an face-centered-cubic (fcc) lattice structure with a lattice constant double of the original cubic one. Many ordered double perovskites incorporate strong intrinsic SOC, as B' ions are commonly $4d$ and $5d$ transition metals. Moreover, the large B'-B' separation weakens exchange, similarly to $FeSc_2S_4$. Here, we construct an appropriate microscopic model for the most quantum of these materials (a list may be found in Table I), in which the magnetic ion contains a single unpaired $S=1/2$ spin.

The physics is strongly influenced by the combination of the orbital degeneracy of the t_{2g} multiplet, which acts as an effective $\ell=1$ orbital angular moment. Due to strong SOC, this combines with the $S=1/2$ spin to induce an effective total angular momentum $j=3/2$ description of the system. Moreover, due to the orbitally dependent exchange, the interaction of these $j=3/2$ contains large biquadratic (fourth order in spin operators) and triquadratic (sixth order in spin operators) interactions. These support exotic phases not easily found in systems with dominant bilinear spin exchange.

Analysis of the microscopic model shows that the strong SOC enhances quantum fluctuations and leads to several in-

TABLE I. A list of ordered double perovskites. Note the discrepancy in Curie-Weiss temperature and μ_{eff} may originate from the experimental fitting of data at different temperature range.

Compound	B' config.	Crystal structure	Θ_{CW} (K)	μ_{eff} (μ_B)	Magnetic transition	Frustration para. f	Ref
Ba_2YMoO_6	$Mo^{5+}(4d^1)$	Cubic	−91	1.34	PM down to 2 K	$f \gtrsim 45$	11
Ba_2YMoO_6	$Mo^{5+}(4d^1)$	Cubic	−160	1.40	PM down to 2 K	$f \gtrsim 80$	12
Ba_2YMoO_6	$Mo^{5+}(4d^1)$	Cubic	−219	1.72	PM down to 2 K	$f \gtrsim 100$	13
La_2LiMoO_6	$Mo^{5+}(4d^1)$	Monoclinic	−45	1.42	Short-range AFM $T_N \sim 20$ K	$f \gtrsim 2$	13
Sr_2MgReO_6	$Re^{6+}(5d^1)$	Tetragonal	−426	1.72	Spin glass, $T_G \sim 50$ K	$f \gtrsim 8$	14
Sr_2CaReO_6	$Re^{6+}(5d^1)$	Monoclinic	−443	1.659	Spin glass, $T_G \sim 14$ K	$f \gtrsim 30$	15
Ba_2CaReO_6	$Re^{6+}(5d^1)$	Cubic to tetragonal (at $T \sim 120$ K)	−38.8	0.744	AFM $T_N = 15.4$ K	$f \sim 2$	16
Ba_2LiOsO_6	$Os^{7+}(5d^1)$	Cubic	−40.48	0.733	AFM $T_N \sim 8$ K	$f \gtrsim 5$	17
Ba_2NaOsO_6	$Os^{7+}(5d^1)$	Cubic	−32.45	0.677	FM $T_N \sim 8$ K	$f \gtrsim 4$	17
Ba_2NaOsO_6	$Os^{7+}(5d^1)$	Cubic	~ -10	~ 0.6	FM $T_N = 6.8$ K	$f \gtrsim 4$	18

teresting phases: (1) an unconventional antiferromagnet (denoted AFM) in which the magnetic *octupole* and *quadrupole* moments rather than the dipole moment are dominant, (2) an unusual noncollinear ferromagnet 110 (denoted FM110) with a doubled unit cell and magnetization along the [110] axis, (3) a (biaxial) "spin nematic" phase with quadrupolar order but unbroken time-reversal symmetry and, more speculatively, (4) a possible quantum-spin-liquid (QSL) phase. Phases (1), (2), and (4) are low-temperature phases and persist as ground states, while the spin nematic, phase (3), occurs in a broad intermediate temperature range below the paramagnetic state but above any magnetic ordering temperature.

States with magnetic multipole order are more often observed in f-electron systems where crystal-field effects are less important than SOC.[19] As a consequence, the atomic wave functions are total angular momentum eigenstates, in which the spin and orbital degrees of freedom are highly entangled. This leads to highly non-Heisenberg exchange between the local moments, which is described by interaction of higher magnetic multipole operators. Such interactions may drive multipolar order, as suggested, for instance, in URu_2Si_2.[20] Recently this has been suggested to also occur in d-electron systems with unquenched orbital degeneracy and sufficient SOC.[21] We find a similar mechanism at work in the AFM phase.

A ferromagnetic state is not in itself unusual, though such is relatively uncommon in insulators. However, cubic ferromagnets with an easy axis oriented along the [110] direction is quite uncommon. This can be understood from the Landau theory for a ferromagnet: the usual fourth-order cubic anisotropy term favors either [100] or [111] orientation, depending upon its sign, but never [110]. To obtain a [110] easy axis, one requires sixth-order or higher terms to be substantial, making this rare indeed. Remarkably, such [110] anisotropy has been observed in experiments on Ba_2NaOsO_6.[18]

Both the above states, when heated above their magnetic ordering temperatures, allow on symmetry grounds for an intermediate phase which is time-reversal symmetric but with quadrupolar order—the spin nematic. Applying the mean-field theory (MFT) at $T > 0$, we indeed find such a phase in a broad range of parameter space. While spin nematic states have been suggested previously in $NiGa_2S_4$,[22–26] it has not been established in that material. The mechanism for quadrupolar order here is much more transparent and robust than in that case.

The above three phases, while somewhat unconventional, may be obtained within a mean-field analysis. A QSL state, however, cannot be described by any mean-field theory, and is considerably more exotic. The search for a QSL, which is a state in which quantum fluctuations prevent spins from ordering even at zero temperature, is a long-standing problem in fundamental physics.[27] Since the possibility of a QSL was suggested by Anderson in the early 1970s,[28] this has been an active area for theory and experiment. Despite the current maturity of the theory for QSL,[29] the experimental confirmation of the existence of such an exotic phase is still elusive. Very commonly geometrical frustration is thought to be a driving mechanism for QSL formation, and consequently most research (both theoretically and experimentally) has been devoted to systems of this type, such as triangular,[30] kagome,[31] hyperkagome,[3,32,33] and pyrochlore lattices.[34]

Here we suggest a different route, in which quantum fluctuations are enhanced primarily by strong SOC, rather than geometrical frustration.[35] In fact, the magnetic ions in ordered double perovskites reside on a fcc sublattice, which can be viewed as edge-sharing tetrahedra, and is somewhat geometrically frustrated. Without strong SOC, however, this frustration is weak, and indeed the classical Heisenberg antiferromagnet on the fcc lattice is known to magnetically order into a state with the ordering wave vector $2\pi(001)$.[36] The tendency of the simple fcc antiferromagnet to order may be partially attributed to its large coordination number ($z = 12$), which leads to mean-fieldlike behavior. By contrast, strong SOC induces effective exchange interactions very different from Heisenberg type, with strong directional dependence that may make a QSL more favorable. To make this suggestion more concrete, we propose a natural wave function for a QSL in our model, and discuss the physical properties of such a state.

We now outline the main results of the paper, and how they are presented in the following sections. In Sec. II, we

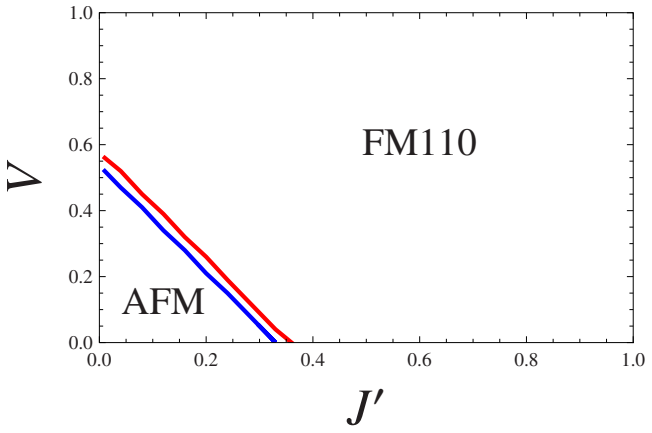

FIG. 1. (Color online) Mean-field $T=0$ phase diagram for the model Hamiltonian in Eq. (27). AFM denotes the "antiferromagnetic" ground state given by Eqs. (39) and (40), FM110 denotes the ferromagnetic ground state with an easy axis oriented along [110], given by Eq. (51). The FM100 state, which is ferromagnetic with easy axis along [100] appears in the narrow band between the two phase boundaries. In the figure, $J=1$.

show that strong SOC leads to an effective $j=3/2$ local moment on each B' site. We write down a model Hamiltonian which includes three interactions: nearest-neighbor (NN) AFM exchange, J, NN FM exchange, J', and electric quadrupolar interaction, V. These interactions are all *projected* down to the effective $j=3/2$ manifold, which induces many terms beyond the usual quadratic exchange. Indeed, because of the four-dimensional basis of spin-3/2 states, the resulting Hamiltonian can be thought of as an anisotropic Γ matrix model.[37] We then discuss the symmetry properties of the projected Hamiltonian. Surprisingly, we find that, in the limit of vanishing FM exchange, the Hamiltonian has a "hidden" global SU(2) symmetry despite its complicated appearance.

In Sec. III, we consider the mean-field ground states of the model, characterized by local (single-site) order parameters. In Sec. III A we begin by considering the more accessible limit in which strong uniaxial single-site anisotropy (due, e.g., to a tetragonal distortion of the crystal) lifts the "orbital" fourfold degeneracy of $j=3/2$ quadruplets down to easy-axis or easy-plane Kramer's doublets. In these limits, the effective Hamiltonian in the reduced phase space is mapped onto that of an XXZ antiferromagnet which can be understood even without mean field theory. Next, in Sec. III B, we carry out $T=0$ mean-field theory for the case of cubic symmetry. Here we find the AFM state and two ferromagnetic states (the FM110 state and another state with a [100] easy axis). The $T=0$ mean-field phase diagram is shown in Fig. 1. Finally, having described the situations with strong and vanishing single-site anisotropy, we determine in Sec. III C the mean-field phase diagram for intermediate anisotropy.

In Sec. IV we identify the multipolar order parameters of the three ordered phases and analyze the $T>0$ behavior by mean-field theory. Here we find the quadrupolar phase and discuss several phase transitions which occur. We also discuss the behavior of the magnetic susceptibility in different parameter regimes.

In Sec. V, we consider quantum effects beyond the mean-field theory. First, we carry out a spin-wave calculation, which determines the collective mode structure, and also shows that in the regime where nearest-neighbor antiferromagnetic exchange is dominant (small J' and V) quantum fluctuations are large and may destabilize the ordered AFM phase. Therefore, we consider possible nonmagnetic ground states, both of valence-bond solid (VBS) and QSL type. We formulate a slave-fermion theory with four-component spin $S=3/2$ fermions, in such a way that at mean-field level the hidden SU(2) symmetry is preserved and the correct ground state, the analog of a singlet in the usual Heisenberg model, is obtained for a single pair of nearest-neighbor sites. The corresponding mean-field theory naturally includes the intrinsic spatial anisotropy of the strong SOC limit. We analyze two different mean-field ansatze with zero and π flux. In both cases the mean-field Hamiltonian respects all the symmetries of the original spin Hamiltonian. The π-flux state is found to have lower mean-field energy. For both states, the spinons are at quarter filling, leading to a spinon Fermi sea. There is no Fermi-surface nesting and we expect that this spinon Fermi surface should be stable against weak perturbations. Predictions based on the picture of spinon Fermi surface are made. Finally in Sec. VI, we compare our theoretical prediction with current experimental findings and suggest further directions for theory and experiment.

II. MODEL AND SYMMETRY

A. Spin-orbit interaction and hybridization of atomic orbitals

The magnetic ions B' (Os^{7+}, Re^{6+}, and Mo^{5+}) found in the ordered double perovskites in Table I all have one electron in the triply degenerate t_{2g} multiplet. The atomic spin-orbit interaction projected down to the t_{2g} triplet is written as

$$\mathcal{H}_{\rm so} = -\lambda \boldsymbol{l}\cdot\boldsymbol{S}, \tag{1}$$

in which the total angular momentum quantum numbers of these operators are $l=1$, $S=1/2$. The effective orbital angular momentum $\boldsymbol{l}$ comes from the projection of orbital angular momentum $\boldsymbol{L}$ onto the t_{2g} triplets,

$$\mathcal{P}_{t_{2g}}\boldsymbol{L}\mathcal{P}_{t_{2g}} = -\boldsymbol{l}. \tag{2}$$

Here $\mathcal{P}_{t_{2g}}=\Sigma_{a=yz,xz,xy}|a\rangle\langle a|$ is the projection operator to the t_{2g} manifold. The eigenstates of l^z with eigenvalues $m=0,\pm 1$ and S^z with eigenvalues $\sigma=\pm 1/2\equiv\uparrow,\downarrow$, written in terms of the usual t_{2g} states are

$$|0,\sigma\rangle = |d^\sigma_{xy}\rangle, \quad |\pm 1,\sigma\rangle = \frac{\mp|d^\sigma_{yz}\rangle - i|d^\sigma_{xz}\rangle}{\sqrt{2}}. \tag{3}$$

This interaction favors $j=3/2$ ($\boldsymbol{j}=\boldsymbol{l}+\boldsymbol{S}$) quadruplets over $j=1/2$ doublets by an energy separation $3\lambda/2$. In the strong spin-orbit interaction limit, the local Hilbert space is restricted to four low-lying states

$$|d_\alpha\rangle = \sum_{m,\sigma} C^\alpha_{m\sigma}|m,\sigma\rangle, \tag{4}$$

where $\alpha=\pm 3/2,\pm 1/2$ is the j^z eigenvalue and

$$C^{\alpha}_{m\sigma} = \left\langle l = 1, S = \frac{1}{2}; m, \sigma \middle| l = 1, S = \frac{1}{2}; j = \frac{3}{2}, \alpha \right\rangle \tag{5}$$

is a Clebsch-Gordan coefficient. In the materials under consideration, λ is indeed a very large energy scale (fraction of an electron volt), justifying the strong SOC limit.

Every operator expressed in terms of spin and orbitals must therefore be projected into this subspace and its projection can be written in terms of $j=3/2$ angular momentum operator. For example,

$$\mathcal{P}_{3/2} \boldsymbol{S} \mathcal{P}_{3/2} = \frac{1}{3} \boldsymbol{j}, \tag{6}$$

$$\mathcal{P}_{3/2} \boldsymbol{l} \mathcal{P}_{3/2} = \frac{2}{3} \boldsymbol{j}. \tag{7}$$

Here $\mathcal{P}_{3/2}$ is the projection operator into the $j=3/2$ quadruplets. Furthermore, for the magnetic moment $\boldsymbol{M}$ for electrons in atomic d orbitals, we have

$$\boldsymbol{M} \equiv \mathcal{P}_{3/2}[2\boldsymbol{S} + (-\boldsymbol{l})]\mathcal{P}_{3/2} = 0. \tag{8}$$

The vanishing magnetic moment is quite remarkable and partially explains why the compounds have small magnetic moments in comparison with spin-$\frac{1}{2}$ systems without orbital degeneracy.

In reality, the measured magnetic moments are nonzero because the atomic $4d$ or $5d$ orbitals strongly hybridize with p orbitals at the oxygen sites that form an octahedron surrounding each B' site. For instance, for Ba_2NaOsO_6, the hybridization energy is estimated to be of the order of electron volts[18,38] and comparable to the energy gap between Os d and O p states. For this reason, it is more appropriate to think in terms of molecular orbitals with mixed d and p character. For example, molecular xy orbitals are written as

$$|D^{\sigma}_{i,xy}\rangle = \frac{|d^{\sigma}_{i,xy}\rangle + r|p^{\sigma}_{i,xy}\rangle}{\sqrt{1+r^2}}, \tag{9}$$

where $|d^{\sigma}_{i,xy}\rangle$ is the state corresponding to one electron in the xy orbital and spin σ on site i, and $|p^{\sigma}_{i,xy}\rangle$ is a linear combination (with xy symmetry) of states that have a singlet on the d_{xy} orbital and one hole on an oxygen site,

$$|p^{\sigma}_{i,xy}\rangle = \frac{1}{2}(|p^{\sigma}_{i+\hat{e}_x,y}\rangle + |p^{\sigma}_{i+\hat{e}_y,x}\rangle + |p^{\sigma}_{i-\hat{e}_x,y}\rangle + |p^{\sigma}_{i-\hat{e}_y,x}\rangle), \tag{10}$$

where $\hat{e}_{x,y}$ are real-space vectors from the B' site to neighboring oxygen along x or y directions. The mixing parameter r is of order t_{dp}/Δ, where t_{dp} is the hopping matrix element between d and p orbitals and Δ is the gap to oxygen p states. In the limit of strong spin-orbit interaction, we must project into four low-lying molecular orbitals which are a superposition of the four atomic states with $j=3/2$ and p states

$$|D_{i,\alpha}\rangle = \sum_{m,\sigma} C^{\alpha}_{m\sigma} |D^{\sigma}_{i,m}\rangle. \tag{11}$$

While the atomic magnetic moment in Eq. (8) vanishes, there is a nonzero contribution to the molecular $\boldsymbol{M}$ from holes in p orbitals. After taking the projection into $j=3/2$ states, the coupling of the molecular orbital to a magnetic field reads

$$\mathcal{H}_Z = -g\mu_B \boldsymbol{h} \cdot \boldsymbol{j}, \tag{12}$$

where $g=r^2/[3(1+r^2)]$ is the Landé factor and μ_B is the Bohr magneton.

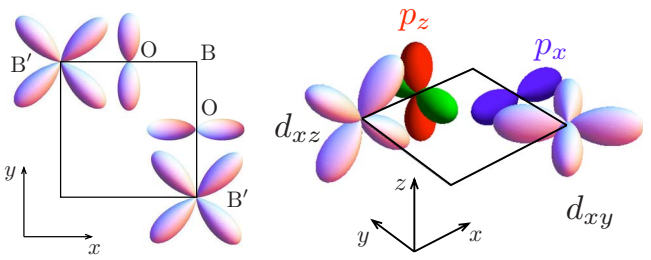

FIG. 2. (Color online) Left graph: the NN AFM exchange path (B'-O-O-B'); right graph: The NN FM exchange path with intermediate orthogonal p orbitals at O sites.

B. Exchange interactions and electric quadrupolar interaction

In the last section, we discussed the effect of strong spin-orbit interaction in determining the local degrees of freedom and pointed out that every operator must be projected into the $j=3/2$ quadruplets. In this section, we introduce the interactions between the local moments and discuss the mechanics of the projection.

The first interaction to consider is nearest-neighbor antiferromagnetic exchange, through the virtual transfer of electrons through intermediate oxygen p orbitals. These processes are strongly restricted by symmetry. For example, in XY planes, only electrons residing on d_{xy} orbitals can virtually hop to neighboring sites via p_x and p_y orbitals of the intermediate oxygen sites. The exchange path and relevant orbitals are depicted in Fig. 2. Alternatively, one can interpret this process as kinetic exchange between molecular D_{xy} orbitals, which are mixtures of the transition metal d state and p states on the neighboring four oxygen [see Eq. (9)]. As a consequence, the antiferromagnetic exchange interaction can be written $\mathcal{H}_{\text{ex-1}} = \mathcal{H}^{\text{XY}}_{\text{ex-1}} + \mathcal{H}^{\text{YZ}}_{\text{ex-1}} + \mathcal{H}^{\text{XZ}}_{\text{ex-1}}$, where

$$\mathcal{H}^{\text{XY}}_{\text{ex-1}} = J \sum_{\langle ij \rangle \in \text{XY}} \left(\boldsymbol{S}_{i,xy} \cdot \boldsymbol{S}_{j,xy} - \frac{1}{4} n_{i,xy} n_{j,xy} \right), \tag{13}$$

where the sum is over nearest-neighbor sites in the XY planes, and the corresponding terms for YZ and XZ planes are obtained by the obvious cubic permutation. Here the operators $\boldsymbol{S}_{i,xy}$ and $n_{i,xy}$ denote the spin residing on xy orbital and orbital occupation number at site i, respectively. In terms of spin and orbital angular momentum operators acting on site i,

$$\boldsymbol{S}_{i,xy} = \boldsymbol{S}_i[1 - (l^z_i)^2], \tag{14}$$

$$n_{i,xy} = 1 - (l^z_i)^2, \tag{15}$$

Throughout this paper, we use the subindices (i,xy) to denote the site and orbitals, superindex $(\mu = x,y,z)$ to denote the spin component, and capital letters (XY, XZ, YZ) to denote the planes. With these definitions, we note that the

single occupancy condition at each site, which defines the Mott insulating state, becomes

$$n_{i,xy} + n_{i,xz} + n_{i,yz} = 1. \tag{16}$$

Moreover, from Eq. (15), orbitally resolved spins satisfy

$$\boldsymbol{S}_{i,xy} + \boldsymbol{S}_{i,yz} + \boldsymbol{S}_{i,xz} = \boldsymbol{S}_i. \tag{17}$$

The second interaction is the nearest-neighbor ferromagnetic exchange interaction. This interaction is due to the spin transfer through orthogonal orbitals at the intermediate oxygen sites in the exchange path, as shown in Fig. 2. For two sites i,j in the XY plane, this ferromagnetic exchange is written as

$$\mathcal{H}^{\mathrm{XY}}_{\text{ex-2},ij} = -J'[\boldsymbol{S}_{i,xy} \cdot (\boldsymbol{S}_{j,yz} + \boldsymbol{S}_{j,xz}) + \langle i \leftrightarrow j \rangle] - \frac{3J'}{4}[n_{i,xy}(n_{j,xz} + n_{j,yz}) + \langle i \leftrightarrow j \rangle], \tag{18}$$

where the xy orbital only interacts with yz and xz orbitals at neighboring sites. Applying the single-occupancy constraint, the nearest-neighbor ferromagnetic exchange interaction can be simplified, up to a constant, to

$$\mathcal{H}^{\mathrm{XY}}_{\text{ex-2}} = -J' \sum_{\langle ij \rangle \in \mathrm{XY}} [\boldsymbol{S}_{i,xy} \cdot (\boldsymbol{S}_{j,yz} + \boldsymbol{S}_{j,xz}) + \langle i \leftrightarrow j \rangle] + \frac{3J'}{2} \sum_{\langle ij \rangle} n_{i,xy} n_{j,xy}. \tag{19}$$

Microscopically, $J'/J \sim \mathcal{O}(J_H/U_p)$, where J_H and U_p are the Hund's coupling and Hubbard Coulomb interaction at the oxygen site, respectively.

The third interaction is the electric quadrupole-quadrupole interaction. The $4d$ or $5d$ electron carries an electric quadrupole moment, and the interaction between these moments may not be negligible because of the long spatial extent of the molecular orbitals. Calculating the direct electrostatic energy between all possible orbital configurations for two electrons residing in neighboring sites in an XY plane, we obtain the quadrupole-quadrupole interaction,

$$\mathcal{H}^{\mathrm{XY}}_{\text{quad},ij} = V n_{i,xy} n_{j,xy} - \frac{V}{2}[n_{i,xy}(n_{j,yz} + n_{i,xz}) + (i \leftrightarrow j)] - \frac{13V}{12}(n_{i,yz} n_{j,yz} + n_{i,xz} n_{j,xz}) + \frac{19V}{12}(n_{i,yz} n_{j,xz} + n_{i,xz} n_{j,yz}). \tag{20}$$

Here $V > 0$ is defined as the Coulomb repulsion between two nearest-neighbor xy orbitals on XY planes. If Q is the magnitude of the electric quadrupole and a is the lattice constant of the fcc lattice, we have $V = 9\sqrt{2}Q^2/a^5$. In general, the main contribution to Q comes from the charge at the oxygen sites, hence the larger the hybridization, the larger the value of V. Using the single-occupancy constraint in Eq. (16) and summing over sites, the quadrupole-quadrupole interaction simplifies to

$$\mathcal{H}^{\mathrm{XY}}_{\text{quad}} = \sum_{\langle ij \rangle \in \mathrm{XY}} \left[-\frac{4V}{3}(n_{i,xz} - n_{i,yz})(n_{j,xz} - n_{j,yz}) + \frac{9V}{4} n_{i,xy} n_{j,xy} \right], \tag{21}$$

in which we have ignored an unimportant constant.

The minimal Hamiltonian for the cubic system contains all three of these exchange interactions in addition to the on-site SOC,

$$\mathcal{H} = \mathcal{H}_{\text{ex-1}} + \mathcal{H}_{\text{ex-2}} + \mathcal{H}_{\text{quad}} + \mathcal{H}_{\text{so}}. \tag{22}$$

Since we are interested in the limit of strong spin-orbit interaction, we need to project $\mathcal{H}$ onto the $j=3/2$ quadruplets at every site. As an example, we write down the projection for $\boldsymbol{S}_{i,xy}$ and $n_{i,xy}$,

$$\tilde{S}^x_{i,xy} = \frac{1}{4} j^x_i - \frac{1}{3} j^z_i J^x_i j^z_i, \tag{23}$$

$$\tilde{S}^y_{i,xy} = \frac{1}{4} j^y_i - \frac{1}{3} j^z_i J^y_i j^z_i, \tag{24}$$

$$\tilde{S}^z_{i,xy} = \frac{3}{4} j^z_i - \frac{1}{3} j^z_i J^z_i j^z_i, \tag{25}$$

$$\tilde{n}_{i,xy} = \frac{3}{4} - \frac{1}{3}(j^z_i)^2, \tag{26}$$

in which, $\tilde{\mathcal{O}} \equiv \mathcal{P}_{3/2} \mathcal{O} \mathcal{P}_{3/2}$. Spin and occupation number operators for other orbitals can be readily generated by a cubic permutation. After the projection, the minimal Hamiltonian reduces, up to a constant, to

$$\tilde{\mathcal{H}} = \tilde{\mathcal{H}}_{\text{ex-1}} + \tilde{\mathcal{H}}_{\text{ex-2}} + \tilde{\mathcal{H}}_{\text{quad}}. \tag{27}$$

As one may notice, the projected Hamiltonian contains four-spin and six-spin interactions in addition to the usual quadratic two-spin interactions if it is expressed in terms of the effective spin moment $\boldsymbol{j}_i$. One can view these multiple spin terms as the interaction between magnetic multipoles (quadrupole and octupole) at different sites. Such multipolar Hamiltonians are much less familiar than the usual quadratic exchange forms and some caution should be used. In particular, experience with similar models shows that such interactions can magnify quantum effects, for instance, leading to the appearance of a quadrupolar phase in the biquadratic case.[23] Hence, the naive classical approximation—replacing $\boldsymbol{j}$'s by classical vectors—is inadvisable, and we will proceed differently below.

C. Symmetry properties of the Hamiltonian

Before we move on to discuss the ground state of the Hamiltonian $\tilde{\mathcal{H}}$ in Eq. (27), we need to have some understanding about its symmetry properties. We start from the NN AFM exchange interaction $\tilde{\mathcal{H}}_{\text{ex-1}}$. The latter has an apparent cubic space-group symmetry. The total angular mo-

mentum $\boldsymbol{J}=\Sigma \boldsymbol{j}_i$ is *not* conserved, $[\tilde{\mathcal{H}}_{\text{ex-1}},\boldsymbol{J}]\neq 0$. Nevertheless, $\tilde{\mathcal{H}}_{\text{ex-1}}$ surprisingly has a hidden SU(2) symmetry. The three generators of this global *continuous* symmetry are defined as follows:

$$G^{\mu}=\sum_i G_i^{\mu}=\sum_i\left[\frac{7}{6}j_i^{\mu}-\frac{2}{3}(j_i^{\mu})^3\right] \tag{28}$$

with $\mu=x,y,z$. One can readily check that these generators commute with $\tilde{\mathcal{H}}_{\text{ex-1}}$,

$$[G^{\mu},\tilde{\mathcal{H}}_{\text{ex-1}}]=0, \tag{29}$$

and satisfy the SU(2) algebra,

$$[G^{\mu},G^{\nu}]=i\epsilon_{\mu\nu\lambda}G^{\lambda}. \tag{30}$$

In addition, the Casimir operator $\mathbf{G}^2$ also commutes with $\tilde{\mathcal{H}}_{\text{ex-1}}$. The physical meaning of these generators is easy to see if one expresses $G^{x,y,z}$ in matrix form. For a single site,

$$G_i^x=-\frac{1}{2}\begin{bmatrix} & & & 1\\ & & 1 & \\ & 1 & & \\ 1 & & & \end{bmatrix}=\frac{1}{2}(-\sigma^x)_{14}\oplus(-\sigma^x)_{23}, \tag{31}$$

$$G_i^y=\frac{1}{2}\begin{bmatrix} & & & -i\\ & & i & \\ & -i & & \\ i & & & \end{bmatrix}=\frac{1}{2}(\sigma^y)_{14}\oplus(-\sigma^y)_{23}, \tag{32}$$

$$G_i^z=\frac{1}{2}\begin{bmatrix} -1 & & & \\ & 1 & & \\ & & -1 & \\ & & & 1 \end{bmatrix}=\frac{1}{2}(-\sigma^z)_{14}\oplus(\sigma^z)_{23}, \tag{33}$$

in which the empty matrix entries are zero and we have expressed these generators as the direct sum of two Pauli matrices, one $(\boldsymbol{\sigma}_{14})$ for the subspace of $j_i^z=\pm 3/2$ states and the other $(\boldsymbol{\sigma}_{23})$ for the subspace of $j_i^z=\pm 1/2$ states. One intuitive way to think about these SU(2) generators is that they transform the spin components in the $j_i^z=\pm 3/2$ subspace together with $j_i^z=\pm 1/2$ subspace. This is a global symmetry of $\tilde{\mathcal{H}}_{\text{ex-1}}$.

Now we consider the other two interactions, $\tilde{\mathcal{H}}_{\text{ex-2}}$ and $\tilde{\mathcal{H}}_{\text{quad}}$. We find that the electric quadrupole-quadrupole interaction $\tilde{\mathcal{H}}_{\text{quad}}$ also commutes with $\mathbf{G}$. On the other hand, the ferromagnetic exchange interaction $\tilde{\mathcal{H}}_{\text{ex-2}}$ breaks this SU(2) symmetry; thus

$$[\tilde{\mathcal{H}},\mathbf{G}]\propto J'. \tag{34}$$

For $J'\ll J,V$, we have an approximate continuous symmetry.

III. MEAN-FIELD GROUND STATES

In this section, we study the ground state of the model Hamiltonian $\tilde{\mathcal{H}}$ in Eq. (27). We begin in Sec. III A by getting some intuition from considering a perturbed model with strong easy-axis or easy-plane anisotropy. This starting point also has experimental motivation as several ordered double perovskites in Table I develop such anisotropies that are driven by lattice distortions. Armed with the understanding of the anisotropic cases, we proceed to analyze the case of cubic symmetry using mean-field theory in Sec. III B. We consider briefly intermediate strength anisotropy in Sec. III C.

In general, Curie-Weiss mean-field theory consists of decoupling all intersite interactions to obtain self-consistent single-site Hamiltonians. At zero temperature, this is equivalent to assuming a product form for the wave function, i.e.,

$$|\Psi\rangle=\otimes_i|\psi_i\rangle, \tag{35}$$

where the product is over sites and $|\psi_i\rangle$ is an arbitrary $j=3/2$ ket. One calculates the mean-field ground-state energy as the expectation value of the Hamiltonian in this state and minimizes it. Thus the mean-field approximation can also be considered as a simple variational one.

A. Case with strong anisotropy

In this section, we add to the Hamiltonian $\tilde{\mathcal{H}}$ in Eq. (27) a strong anisotropic term,

$$\mathcal{H}_{\text{ani}}=-D\sum_i(j_i^z)^2, \tag{36}$$

in which, D can be positive or negative, representing easy-axis or easy-plane anisotropy, respectively. Although this interaction is anisotropic in spin space, it still respects the hidden global SU(2) symmetry.

1. Easy-axis anisotropy

Let us start with easy-axis anisotropy $D>0$. Assuming the anisotropy is very strong $D\gg J,J',V$ and $D\ll\lambda$, which favors $j_i^z=\pm 3/2$ states, we can safely project the Hamiltonian $\tilde{\mathcal{H}}$ into the latter two-dimensional (2D) subspace. We then obtain the effective Hamiltonian

$$\mathcal{H}_{\text{eff-1}}=\sum_{\langle ij\rangle\in\text{XZ,YZ}}\left[\left(\frac{J}{4}+\frac{J'}{2}\right)\boldsymbol{T}_i\cdot\boldsymbol{T}_j-J'T_i^zT_j^z\right]+\mathcal{N}\left(-\frac{J}{4}+\frac{3J'}{2}+\frac{11V}{12}\right), \tag{37}$$

where we have introduced pseudospin-1/2 operators $\boldsymbol{T}_i$ acting on the basis $j_i^z=\pm 3/2$ with $T_i^z=\pm 1/2$ corresponding to $j_i^z=\pm 3/2$, respectively. And $\mathcal{N}$ is the total number of sites. In the reduced space, the original spin vector reduces to the pseudospin in the following way:

$$(j^x,j^y,j^z)\Rightarrow 3(0,0,T^z). \tag{38}$$

Notice that after this projection the interaction on the horizontal bonds in XY planes disappear in the effective Hamiltonian $\mathcal{H}_{\text{eff-1}}$. This can be understood in terms of the original orbital picture as the easy-axis anisotropy lifts the degeneracy of t_{2g} triplets, favoring xz and yz orbitals to be occu-

pied. As a result, *the above effective Hamiltonian is operating on a bond-depleted fcc lattice, which is in fact a unfrustrated bipartite bcc lattice*.

In $\mathcal{H}_{\text{eff-1}}$ because of the in-plane anisotropy introduced by the FM exchange, the ground state of $\mathcal{H}_{\text{eff-1}}$ is "antiferromagnetically" ordered in the (T^x, T^y) plane with an ordering wave vector $\boldsymbol{Q}=2\pi(001)$. We denote this as the AFM state. The corresponding mean-field ground state is just the direct product,

$$|\Psi(\phi)\rangle = \prod_i |\psi_i(\phi)\rangle, \tag{39}$$

where

$$|\psi_i(\phi)\rangle = \frac{1}{\sqrt{2}}\left[\left|j_i^z=\frac{3}{2}\right\rangle + (-)^{2z_i}e^{i\phi}\left|j_i^z=\frac{3}{2}\right\rangle\right] \tag{40}$$

with an arbitrary phase ϕ. The arbitrariness of the phase comes from the U(1) symmetry of the projected effective Hamiltonian Eq. (37). However, as discussed in the previous section, the continuous symmetry in the original Hamiltonian is broken completely when $J' \neq 0$. Therefore, the U(1) symmetry of Hamiltonian in Eq. (37) is a by-product of the projection. Because we are in the subspace of $j^z=\pm 3/2$, the orbital occupation is

$$(\langle\tilde{n}_{i,yz}\rangle, \langle\tilde{n}_{i,xz}\rangle, \langle\tilde{n}_{i,xy}\rangle) = (1/2, 1/2, 0). \tag{41}$$

It is also important to note that the ground state in Eq. (40) is not a conventional Néel state as it has a vanishing static magnetic dipole moment,

$$\langle\Psi|\boldsymbol{j}_i|\Psi\rangle = 0. \tag{42}$$

The ϕ dependence only shows up in the spin operators of a specific orbital,

$$\langle\Psi|\tilde{\boldsymbol{S}}_{i,yz}|\Psi\rangle = -\frac{1}{4}(-)^{2z_i}(\cos\phi, \sin\phi, 0), \tag{43}$$

$$\langle\Psi|\tilde{\boldsymbol{S}}_{i,xz}|\Psi\rangle = \frac{1}{4}(-)^{2z_i}(\cos\phi, \sin\phi, 0), \tag{44}$$

$$\langle\Psi|\tilde{\boldsymbol{S}}_{i,xy}|\Psi\rangle = (0,0,0). \tag{45}$$

2. Easy-plane anisotropy

Now we consider easy-plane anisotropy $D<0$. We also assume the anisotropy is very strong $|D| \gg J, J', V$ and $|D| \ll \lambda$, which favors $j_i^z=\pm 1/2$ states and obtain the effective Hamiltonian after projection into the $j_i^z=\pm 1/2$ subspace,

$$\mathcal{H}_{\text{eff-2}} = \sum_{\langle ij\rangle\in \text{XY}} \frac{4}{9}(J\boldsymbol{T}_i\cdot\boldsymbol{T}_j + J' T_i^z T_j^z) + \sum_{\langle ij\rangle\in \text{XZ}}\left[\frac{J}{36}\boldsymbol{T}_i\cdot\boldsymbol{T}_j + J' \times\left(-\frac{1}{6}T_i^x T_j^x + \frac{5}{18}T_i^y T_j^y + \frac{1}{6}T_i^z T_j^z\right)\right] + \sum_{\langle ij\rangle\in \text{YZ}}\left[\frac{J}{36}\boldsymbol{T}_i\cdot\boldsymbol{T}_j + J'\left(\frac{5}{18}T_i^x T_j^x - \frac{1}{6}T_i^y T_j^y + \frac{1}{6}T_i^z T_j^z\right)\right] + \mathcal{N}\left(-\frac{J}{4}+\frac{3J'}{2} + \frac{11V}{12}\right). \tag{46}$$

Here the pseudospin-1/2 operator $\boldsymbol{T}$ is acting on the subspace of $j^z=\pm 1/2$ with $T^z=\pm 1/2$ representing $j^z=\pm 1/2$, respectively. In the reduced spin space, the original spin vector is reduced to the pseudospin in the following way:

$$(j^x, j^y, j^z) \Rightarrow (2T^x, 2T^y, T^z). \tag{47}$$

We can now find the mean-field ground state of this Hamiltonian. For an effective $S=1/2$ model of this type, this is equivalent to the classical approximation. Classically, we can find the minimum-energy states by the Luttinger-Tisza method. This amounts to looking for the eigenvalues of the spin Hamiltonian regarded as a quadratic form and seeking a classical spin solution which is built of a superposition only of those eigenvectors which have minimum-energy eigenvalues. The result in this case is that, for $0<J'<J$, there are two classes of solution, all collinear spin states. These are: (i) states with $\boldsymbol{Q}=2\pi(100)$ and the pseudospin axis in the yz plane, and (ii) states with $\boldsymbol{Q}=2\pi(010)$ and the pseudospin axis in the xz plane. As for the easy-axis case, there is an accidental degeneracy of spin orientations within the plane normal to $\boldsymbol{Q}$. Note that while the pseudospin orients freely along a circle in this plane, the magnetization orients along an ellipse due to the factor of 2 in Eq. (47). One readily expresses the ground state in the unprojected Hilbert space. For example, taking $\boldsymbol{Q}=2\pi(010)$ and pseudospin pointing along x direction, then

$$|\Psi\rangle = \prod_i |\psi_i\rangle \tag{48}$$

with

$$|\psi_i\rangle = \frac{1}{\sqrt{2}}\left[\left|j_i^z=\frac{1}{2}\right\rangle + (-)^{2y_i}\left|j_i^z=-\frac{1}{2}\right\rangle\right]. \tag{49}$$

This is once again an antiferromagnetic state, and to distinguish it from the one which obtains for Ising anisotropy, we denote it AFM′. The defining difference of the AFM′ and the AFM state discussed previously is that, the former has a nonzero dipole moment, while, at least within mean-field theory, the latter does not.

B. Cubic case

Having understood the cases with strong easy-axis and easy-plane anisotropies, let us now turn to the Hamiltonian $\tilde{\mathcal{H}}$ with cubic lattice symmetry in Eq. (27). Both ground states of the Hamiltonian with strong easy-axis or easy-plane anisotropy comprise two-sublattice structure with an ordering wave vector equivalent to $\boldsymbol{Q}=2\pi(001)$. It is therefore natural to guess that the same two-sublattice structure is also obtained in the cubic case. While we have not proven this, we have investigated more general mean-field ground states, allowing for much larger unit cells, but found in every case that the minimum energy is found for the two-sublattice configuration. Therefore, in what follows, we assume the two-sublattice structure with ordering $\boldsymbol{Q}=2\pi(001)$ [which is

equivalent to $2\pi(100)$ and $2\pi(010)$ in the cubic case]. We make no further assumptions and minimize the energy with respect to an arbitrary wave function on each of the two sublattices. The resulting variational phase diagram is depicted in Fig. 1.

1. Antiferromagnetic state

In Fig. 1, for small J'/J and V/J, we find a phase, denoted AFM, which is the natural continuation of the AFM phases encountered in the anisotropic limits. Here, as in those cases, the states on the two sublattices are simply related by a time-reversal transformation, and indeed the ground state has the same form as that found in the easy-axis case, Eqs. (39) and (40). The appearance of time-reversed pairs of sites is natural, since the largest interaction, $\tilde{\mathcal{H}}_{\text{ex-1}}$, is dominated by the spin-spin exchange term. Interestingly, one finds that the ground state has a continuous degeneracy: the phase ϕ in Eq. (40) can be arbitrary. Since the Hamiltonian with nonvanishing J' has no continuous symmetry, this degeneracy appears to be accidental. Since it has the same form as we found in Sec. III A 1, we continue to use the label AFM here for this state (and in Fig. 1).

2. Ferromagnetic 110 state

With large J'/J and V/J, the orbital-orbital interaction has more weight in the Hamiltonian $\tilde{\mathcal{H}}$, and the nature of the ground state changes. One should note that even the pure orbital-orbital interaction is not trivial and classical since the orbital occupation numbers no longer commute after projection down to the $j=3/2$ quadruplets. However, in mean-field theory one may still treat the expectation values classically. Note that the largest terms in the orbital-orbital interaction are those which are diagonal in the orbital basis, namely, the second term in Eq. (19) and the second term in Eq. (21). To minimize the diagonal orbital interaction such as $\tilde{n}_{i,xz}\tilde{n}_{j,xz}$, a schematic recipe is to maximize $\tilde{n}_{i,xz}$ while minimizing $\tilde{n}_{j,xz}$. This is necessary because one cannot minimize both $\tilde{n}_{i,xz}$ and $\tilde{n}_{j,xz}$ simultaneously, since, due to the single-occupancy constraint, the other diagonal terms such as $\tilde{n}_{i,yz}\tilde{n}_{j,yz}$ would then be increased. Since the occupation numbers of the same orbital must be taken different on different sites, and these occupation numbers are time-reversal invariant, the states on the two sublattices cannot be time-reversed counterparts. Consequently, there is a competition between the orbital-orbital interactions ($\tilde{\mathcal{H}}_{\text{ex-2}}$ and $\tilde{\mathcal{H}}_{\text{quad}}$) and the nearest-neighbor antiferromagnetic exchange interaction $\tilde{\mathcal{H}}_{\text{ex-1}}$. In the large J'/J and V/J region, when the orbital interactions dominate, we find however that time-reversal symmetry is still broken, and since these states are not composed of time-reversed pairs, the result is an uncompensated net ferromagnetic moment.

In the majority of phase space, we find the ground state is characterized by three parameters, r, ϕ_1, and ϕ_2,

$$|\psi_A\rangle_{\text{FM110}} = \frac{r}{\sqrt{2}}\left(e^{i\phi_1}\left|j^z=\frac{1}{2}\right\rangle + e^{i(\phi_2-\phi_1)}\left|j^z=-\frac{1}{2}\right\rangle\right) + \sqrt{\frac{1-r^2}{2}}\left(e^{i\phi_2}\left|j^z=\frac{3}{2}\right\rangle + \left|j^z=-\frac{3}{2}\right\rangle\right), \tag{50}$$

$$|\psi_B\rangle_{\text{FM110}} = \frac{r}{\sqrt{2}}\left(-e^{-i\phi_1}\left|j^z=\frac{1}{2}\right\rangle + ie^{i(\phi_1-\phi_2)}\left|j^z=-\frac{1}{2}\right\rangle\right) + \sqrt{\frac{1-r^2}{2}}\left(-ie^{-i\phi_2}\left|j^z=\frac{3}{2}\right\rangle + \left|j^z=-\frac{3}{2}\right\rangle\right), \tag{51}$$

in which, "A" and "B" represent the two sublattices, and r, ϕ_1, and ϕ_2 are determined by minimizing the mean-field energy. Note that in Eq. (51) the three parameters r, ϕ_1, and ϕ_2 are uniquely determined by J'/J and V/J. So the orbital occupations can be readily generated,

$$(\langle\tilde{n}_{A,yz}\rangle,\langle\tilde{n}_{A,xz}\rangle,\langle\tilde{n}_{A,xy}\rangle)_{\text{FM110}} = \left(\frac{1}{2}-\frac{r^2}{3}-\frac{r\sqrt{1-r^2}}{\sqrt{3}}\cos\phi_1,\frac{1}{2}-\frac{r^2}{3}+\frac{r\sqrt{1-r^2}}{\sqrt{3}}\cos\phi_1,\frac{2r^2}{3}\right), \tag{52}$$

$$(\langle\tilde{n}_{B,yz}\rangle,\langle\tilde{n}_{B,xz}\rangle,\langle\tilde{n}_{B,xy}\rangle)_{\text{FM110}} = \left(\frac{1}{2}-\frac{r^2}{3}+\frac{r\sqrt{1-r^2}}{\sqrt{3}}\cos\phi_1,\frac{1}{2}-\frac{r^2}{3}-\frac{r\sqrt{1-r^2}}{\sqrt{3}}\cos\phi_1,\frac{2r^2}{3}\right). \tag{53}$$

It is interesting to see the spin vectors of two sublattices are symmetric about $[1\bar{1}0]$ direction,

$$\langle\boldsymbol{j}_A\rangle_{\text{FM110}} = r[\sqrt{3-3r^2}\cos(\phi_1-\phi_2)+r\cos(2\phi_1-2\phi_2),\sqrt{3-3r^2}\sin(\phi_1-\phi_2)-r\sin(2\phi_1-2\phi_2),0], \tag{54}$$

$$\langle\boldsymbol{j}_B\rangle_{\text{FM110}} = r[-\sqrt{3-3r^2}\sin(\phi_1-\phi_2)+r\sin(2\phi_1-2\phi_2),-\sqrt{3-3r^2}\cos(\phi_1-\phi_2)-r\cos(2\phi_1-2\phi_2),0], \tag{55}$$

so the system has a nonvanishing net spin polarization, that is

$$\frac{1}{2}\langle\boldsymbol{j}_A+\boldsymbol{j}_B\rangle_{\text{FM110}} = \frac{r}{2}\{\sqrt{3-3r^2}[\cos(\phi_1-\phi_2)-\sin(\phi_1-\phi_2)]+r[\cos(2\phi_1-\phi_2)+\sin(2\phi_1-\phi_2)]\}(1,-1,0). \tag{56}$$

This direction of polarization is equivalent to [110] by a 90° rotation, so we denote this a FM110 state. It occupies the corresponding region in Fig. 1.

3. Ferromagnetic 100 (FM100) state

Between the AFM and FM110 states, a narrow region of intermediate phase intervenes (see Fig. 1). Numerically we find this phase is characterized by two parameters r_1 and r_2,

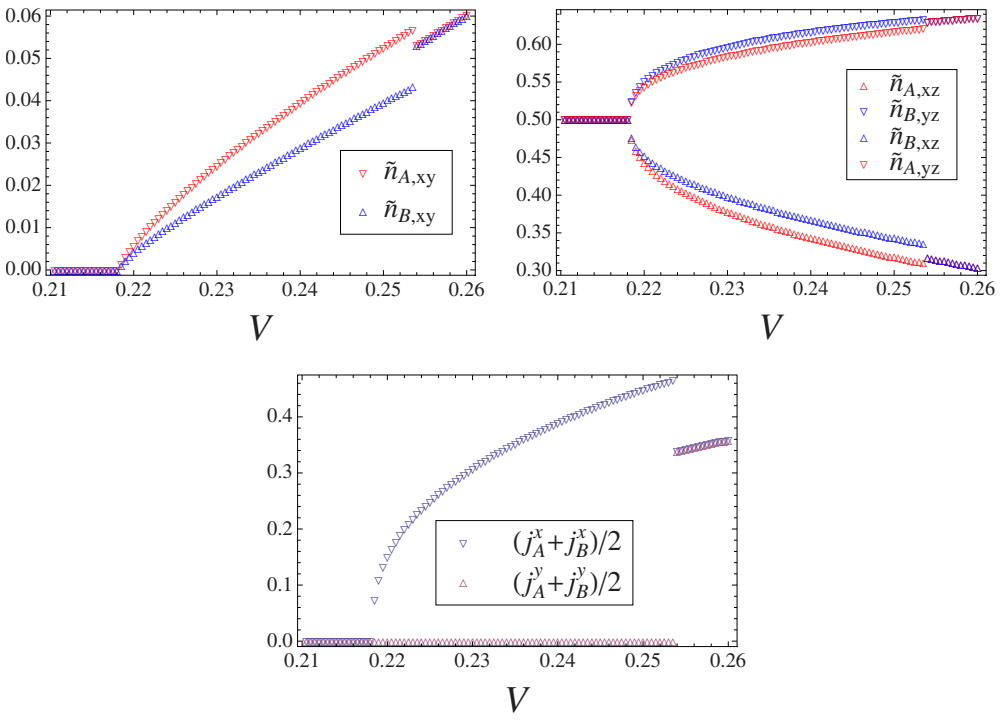

FIG. 3. (Color online) Upper graph: $\tilde{n}_{xy}$ versus V; middle graph: $\tilde{n}_{xz}$ and $\tilde{n}_{yz}$ versus V; and lower graph: the net spin polarization per site versus V. In all three graphs, $J=1$ and $J'=0.2$, and $T=0$. The assignment of A and B sublattices is arbitrary. Here we take the choice given in the text.

$$|\psi_A\rangle_{\mathrm{FM100}} = \frac{r_1}{\sqrt{2}}\left(\left|j^z=\frac{1}{2}\right\rangle + \left|j^z=-\frac{1}{2}\right\rangle\right) + \sqrt{\frac{1-r_1^2}{2}}\left(\left|j^z=\frac{3}{2}\right\rangle + \left|j^z=-\frac{3}{2}\right\rangle\right), \quad (57)$$

$$|\psi_B\rangle_{\mathrm{FM100}} = \frac{r_2}{\sqrt{2}}\left(-\left|j^z=\frac{1}{2}\right\rangle + \left|j^z=-\frac{1}{2}\right\rangle\right) + \sqrt{\frac{1-r_2^2}{2}}\left(-\left|j^z=\frac{3}{2}\right\rangle + \left|j^z=-\frac{3}{2}\right\rangle\right). \quad (58)$$

The parameters r_1 and r_2 are determined by J'/J and V/J and in this intermediate phase $r_1 \neq r_2$. A second ground state is obtained then by interchanging r_1 and r_2. The orbital occupation numbers and spin vectors are given by

$$(\langle\tilde{n}_{A,yz}\rangle,\langle\tilde{n}_{A,xz}\rangle,\langle\tilde{n}_{A,xy}\rangle)_{\mathrm{FM100}} = \left(\frac{1}{2}-\frac{r_1^2}{3}-\frac{r_1}{\sqrt{3}}\sqrt{1-r_1^2},\frac{1}{2}-\frac{r_1^2}{3}+\frac{r_1}{\sqrt{3}}\sqrt{1-r_1^2},\frac{2r_1^2}{3}\right), \quad (59)$$

$$(\langle\tilde{n}_{B,yz}\rangle,\langle\tilde{n}_{B,xz}\rangle,\langle\tilde{n}_{B,xy}\rangle)_{\mathrm{FM100}} = \left(\frac{1}{2}-\frac{r_2^2}{3}+\frac{r_2}{\sqrt{3}}\sqrt{1-r_2^2},\frac{1}{2}-\frac{r_2^2}{3}-\frac{r_2}{\sqrt{3}}\sqrt{1-r_2^2},\frac{2r_2^2}{3}\right), \quad (60)$$

and

$$\langle \boldsymbol{j}_A\rangle_{\mathrm{FM100}} = (r_1^2 + r_1\sqrt{3-3r_1^2},0,0), \quad (61)$$

$$\langle \boldsymbol{j}_B\rangle_{\mathrm{FM100}} = (r_2^2 - r_2\sqrt{3-3r_2^2},0,0). \quad (62)$$

We see that the net spin polarization is along the [100] direction. Due to cubic symmetry, all possible [100] directions are possible. By analogy with the previous phase, we denote this phase FM100. It occupies the narrow region shown in Fig. 1.

4. Transitions

The intermediate FM100 state in Eq. (58) is smoothly connected to the AFM state, which is obtained by setting $r_1=r_2=0$. By contrast, it cannot be connected to the FM110 state. This indicates that the transition between FM100 to AFM is continuous while the transition from FM100 to FM110 is first order. Indeed, this can also be clearly seen from the behavior of the spin and orbital order parameters across these transitions (see Fig. 3). Both the spin and orbital order parameters jump when the system goes from FM100 phase to FM110 phase.

The approach to the line $J'=0$, while not a transition per se, does represent a change in behavior. In particular, on this line, the hidden SU(2) symmetry is restored, and new ground states may be obtained from the above three phases by SU(2) rotations. This allows, for instance, for AFM states to develop with nonvanishing magnetic dipole order in the ground state. However, for arbitrarily small J' the SU(2)-induced degeneracy is broken and the results quoted above hold.

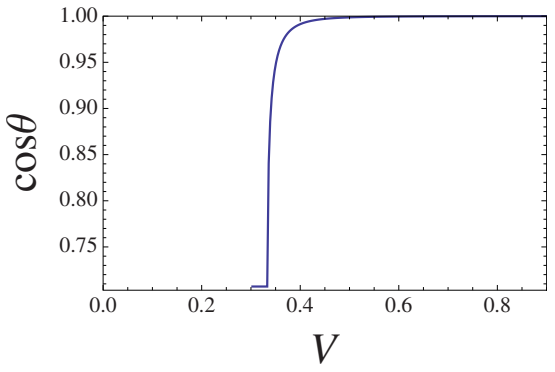

FIG. 4. (Color online) The orientation of the net spin polarization for the FM110* phase, at $T=0$. θ is angle between the net spin polarization and nearest [110] direction. In the figure, $J'=0.2$, $D=-0.05$, $J=1$. $\cos\theta$ increases from $1/\sqrt{2}$ for the FM100 phase to 1 for the FM110* phase as V goes through the phase transition point.

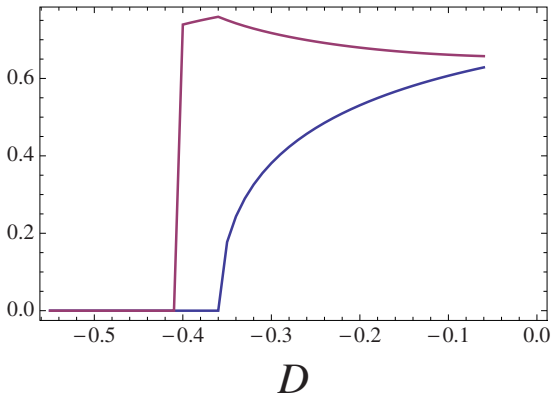

FIG. 5. (Color online) The net polarization versus the easy-plane anisotropy, at $T=0$. The upper curve (in red) is for the y component of the net polarization. And the lower curve (in blue) is for the z component of the net polarization. The ordering wave vector is $\boldsymbol{Q}=2\pi(100)$. In the graph, $J'=V=0.4$ and $J=1$. When $0<|D|\lesssim 0.36$, the system is in FM110* phase; when $0.36<|D|<0.41$, the system is in the FM100 phase; when $|D|\gtrsim 0.41$, the system is in AFM′ phase.

C. Intermediate anisotropy

We briefly address here the evolution of the ground states with increasing $|D|$ between the cubic and strongly anisotropic limits. For easy-axis anisotropy, $D>0$, this process is relatively simple. The AFM phase [with $\boldsymbol{Q}=2\pi(001)$] is favored by this sign of anisotropy, and therefore, with increasing D, it expands at the expense of the FM110 and FM100 states. Indeed, for very large D, ferromagnetic states occur only for unphysically large J' and V.

In the case of easy-plane anisotropy, $D<0$, the phase diagram is more subtle. For weak $|D|$, the main effect is to break the symmetry between the formerly equivalent [100] wave vectors. In this case, states with minimal $\langle j_z^2\rangle$ are favored, which prefers $\boldsymbol{Q}=2\pi(100),2\pi(010)$ rather than $\boldsymbol{Q}=2\pi(001)$.

If we begin in the AFM state for $D=0$, this aligns the pseudospin in the plane normal to this wave vector. The phase degeneracy which obtains for the cubic case is broken by the anisotropy and a definite alignment is obtained. Moreover, as states with $j_z=\pm 1/2$ are increasingly mixed into the ground state, a nonvanishing dipole moment, proportional to the pseudospin, is induced. The magnitude of this staggered magnetization grows continuously with $|D|$, eventually as $D\to-\infty$, approaching the value obtained in Sec. III A 2. This local moment is oriented in the plane normal to $\boldsymbol{Q}$, and can take values distributed over an *ellipse* in this plane. In the large $|D|$ limit, this ratio of the major (perpendicular to $\boldsymbol{Q}$ and to z) and minor (z) axes of the ellipse approaches 2, corresponding to the accidental degeneracy discussed in Sec. III A 2. Because the state for nonzero D evolves smoothly into this limit, and has a nonzero local moment, we denote it an AFM′ state, following the earlier notation.

Beginning in the FM110 state at $D=0$, one observes two subsequent transitions. First, small $|D|$ orients the magnetization normal to $\boldsymbol{Q}$. For concreteness consider $\boldsymbol{Q}=2\pi(100)$, in which case one obtains a ferromagnetic magnetization of the form $\boldsymbol{m}=(0,m_1,m_2)$. For $D=0^-$, $m_1=m_2$, but subsequently m_2 decreases such that $m_2<m_1$. We denote this state FM110*. An example for the orientation of net polarization in the FM110* by varying V is given in Fig. 4. Eventually once some critical anisotropy is reached, m_2 vanishes continuously. At this point the magnetization is aligned along the (010) axis. For yet larger anisotropy, eventually the ferromagnetic magnetization vanishes entirely, and the ground state switches to the AFM′ state. An example of the transitions from FM110* to FM100 then to AFM′ by varying the easy-plane anisotropy D is given in Fig. 5.

Finally, starting in the FM100 state, the magnetization immediately switches to the (010) direction. This is the same phase as the intermediate phase observed starting from the FM110 phase. Thus with further increase in anisotropy, the ground state switches to the AFM′ state.

One may also visualize the evolution of the ground states with anisotropy by considering planar phase diagrams at fixed D. With increasing positive D (Ising anisotropy), the AFM state is stabilized, and simply expands in the J'-V plane, pushing the FM100 and FM110 states outward. For increasing negative D, apart from the fact that the AFM and FM110 states evolve into the AFM′ and FM110* states, the behavior is similar: the AFM′ state expands at the expense of the ferromagnetic states.

IV. MULTIPOLAR ORDERS AND $T>0$ BEHAVIOR

A. Order parameters

In this section, we extend the analysis of the previous section to nonzero temperature. To do so, we employ the usual extension of mean-field theory to include thermal fluctuations. To characterize the phases encountered in this treatment, it is natural to introduce several types of order parameter. First, on a single-site i, we may measure the dipole moment, which is proportional to $\boldsymbol{j}_i$. However, we may also measure the next two multipoles: the quadrupole moment, proportional to

$$Q_i^{\mu\nu}=\langle j_i^\mu j_i^\nu\rangle-\frac{j(j+1)}{3}\delta^{\mu\nu} \tag{63}$$

and the octupole moment

TABLE II. Multipole moments within a cubic Γ_8 quartet. Bars over symbols indicate the sum with respect to all the possible permutations of the indices, e.g., $\overline{j^x(j^y)^2}=j^x(j^y)^2+j^yj^xj^y+(j^y)^2j^x$. Adapted from Refs. 19 and 39.

Moment	Symmetry	Operator
Dipole	Γ_4	$M^x=j^x$
		$M^y=j^y$
		$M^z=j^z$
Quadrupole	Γ_3	$Q^{3z^2}=[3(j^z)^2-\boldsymbol{j}^2]/\sqrt{3}$
		$Q^{x^2-y^2}=(j^x)^2-(j^y)^2$
	Γ_5	$Q^{xy}=\overline{j^xj^y}/2$
		$Q^{yz}=\overline{j^yj^z}/2$
		$Q^{xz}=\overline{j^zj^x}/2$
Octupole	Γ_2	$T_{xyz}=\sqrt{15}/6\overline{j^xj^yj^z}$
	Γ_4	$T^x_\alpha=(j^x)^3-[\overline{j^x(j^y)^2}+\overline{(j^z)^2j^x}]/2$
		$T^y_\alpha=(j^y)^3-[\overline{j^y(j^z)^2}+\overline{(j^x)^2j^y}]/2$
		$T^z_\alpha=(j^z)^3-[\overline{j^z(j^x)^2}+\overline{(j^y)^2j^z}]/2$
	Γ_5	$T^x_\beta=\sqrt{15}[\overline{j^x(j^y)^2}-\overline{(j^z)^2j^x}]/6$
		$T^y_\beta=\sqrt{15}[\overline{j^y(j^z)^2}-\overline{(j^x)^2j^y}]/6$
		$T^z_\beta=\sqrt{15}[\overline{j^z(j^x)^2}-\overline{(j^y)^2j^z}]/6$

$$O_i^{\mu\nu\lambda}=\langle j_i^\mu j_i^\nu j_i^\lambda\rangle. \tag{64}$$

A typical magnetic state has a nonvanishing local dipole moment, which inevitably induces some higher multipole order parameters (see below). However, one sometimes encounters purely multipole states, in which $\langle j_i^\mu\rangle=0$ but $Q_i^{\mu\nu}$ and/or $O_i^{\mu\nu\lambda}$ are/is nonvanishing.

The components of these tensor can be decomposed into irreducible representations of the cubic group (characterizing the symmetry of the ideal double perovskite structure). This decomposition is described fully in Table II. Here we note, in particular, the two-dimensional Γ_3 representation

$$Q_i^{3z^2}=\frac{1}{\sqrt{3}}\langle 3(j_i^z)^2-j(j+1)\rangle,$$

$$Q_i^{x^2-y^2}=\langle (j_i^x)^2-(j_i^y)^2\rangle, \tag{65}$$

which are analogous to the e_g orbitals in atomic physics. The remaining three independent components of $Q_i^{\mu\nu}$ ($j_i^xj_i^y+j_i^yj_i^x$, etc.) form a three-dimensional representation analogous to the t_{2g} orbitals but do not appear in our analysis.

Another important way to break up the tensor order parameters is into combinations which appear in the spin Hamiltonian. Specifically, these are the orbital occupation operators, $\tilde{n}_{i,yz},\tilde{n}_{i,xz},\tilde{n}_{i,xy}$, and the orbitally resolved spin operators, $\tilde{S}^\mu_{i,yz},\tilde{S}^\mu_{i,xz},\tilde{S}^\mu_{i,xy}$. These can be expressed in terms of the multipoles describe above. For the occupation numbers,

$$\tilde{n}_{i,yz}=\frac{1}{3}+\frac{1}{6\sqrt{3}}Q_i^{3z^2}-\frac{1}{6}Q_i^{x^2-y^2},$$

$$\tilde{n}_{i,xz}=\frac{1}{3}+\frac{1}{6\sqrt{3}}Q_i^{3z^2}+\frac{1}{6}Q_i^{x^2-y^2},$$

$$\tilde{n}_{i,xy}=\frac{1}{3}-\frac{1}{3\sqrt{3}}Q_i^{3z^2}. \tag{66}$$

The orbitally resolved spins decompose as

$$\tilde{S}^x_{i,yz}=\frac{1}{15}j_i^x-\frac{2}{15}T^x_{i,\alpha},$$

$$\tilde{S}^y_{i,yz}=\frac{2}{15}j_i^y+\frac{1}{15}T^y_{i,\alpha}+\frac{1}{3\sqrt{15}}T^y_{i,\beta},$$

$$\tilde{S}^z_{i,yz}=\frac{2}{15}j_i^z+\frac{1}{15}T^z_{i,\alpha}-\frac{1}{3\sqrt{15}}T^z_{i,\beta},$$

$$\tilde{S}^x_{i,xz}=\frac{2}{15}j_i^x+\frac{1}{15}T^x_{i,\alpha}-\frac{1}{3\sqrt{15}}T^x_{i,\beta},$$

$$\tilde{S}^y_{i,xz}=\frac{1}{15}j_i^y-\frac{2}{15}T^y_{i,\alpha},$$

$$\tilde{S}^z_{i,xz}=\frac{2}{15}j_i^z+\frac{1}{15}T^z_{i,\alpha}+\frac{1}{3\sqrt{15}}T^z_{i,\beta},$$

$$\tilde{S}^x_{i,xy}=\frac{2}{15}j_i^x+\frac{1}{15}T^x_{i,\alpha}+\frac{1}{3\sqrt{15}}T^x_{i,\beta},$$

$$\tilde{S}^y_{i,xy}=\frac{2}{15}j_i^y+\frac{1}{15}T^y_{i,\alpha}-\frac{1}{3\sqrt{15}}T^y_{i,\beta},$$

$$\tilde{S}^z_{i,xy}=\frac{1}{15}j_i^z-\frac{2}{15}T^z_{i,\alpha}. \tag{67}$$

B. Cubic system: Phases

We first discuss the phases occurring in the cubic system at $T>0$. The ground states discussed earlier are all stable to small thermal fluctuations and hence persist at low temperature. Thus we expect, broadly speaking, an AFM and ferromagnetic (FM110/FM100) region at low temperature. Of course, at temperatures much larger than J, one has a disordered paramagnetic phase. Interestingly, an additional phase appears at intermediate temperature. This is a nonmagnetic *quadrupolar ordered* phase.

To see how this arises, we describe the mean-field procedure and its results. Mean-field theory is formulated in the usual way. We self-consistently decouple interactions between different sites i and j as follows:

$$\hat{\mathcal{O}}_i\cdot\hat{\mathcal{O}}_j\Rightarrow\hat{\mathcal{O}}_i\cdot\langle\hat{\mathcal{O}}_j\rangle+\langle\hat{\mathcal{O}}_i\rangle\cdot\hat{\mathcal{O}}_j-\langle\hat{\mathcal{O}}_i\rangle\cdot\langle\hat{\mathcal{O}}_j\rangle, \tag{68}$$

where $\hat{\mathcal{O}}_i$ and $\hat{\mathcal{O}}_j$ are two operators at site i and j, respectively. These operators are nothing but the orbital occupation numbers and orbitally resolved spins, which are related to the multipolar operators by Eqs. (66) and (67). Decoupling *all* pairwise interactions between sites in this way, we then

obtain a set of single-site problems for each $j=3/2$. Note that these single-site problems involve not just the usual Weiss exchange field, but also "multipolar fields," which act as effective second- and third-order spin anisotropies. The mean-field equations determine self-consistent values of the orbital occupation numbers and orbitally resolved fields. As it is straightforward to formulate the mean-field equations, and solve them numerically, we do not give the details of these calculations here.

A distinct class of solutions describes each phase. For the antiferromagnetic phase, we find the following operators are nonzero:

$$\langle \boldsymbol{j}_i \rangle = \pm n(u_1,u_2,0), \tag{69}$$

$$\langle Q_i^{3z^2} \rangle = q, \tag{70}$$

$$\langle \boldsymbol{T}_{i,\alpha} \rangle = \pm t_\alpha(u_1,u_2,0), \tag{71}$$

$$\langle \boldsymbol{T}_{i,\beta} \rangle = \pm t_\beta(-u_1,u_2,0), \tag{72}$$

where we have taken $\boldsymbol{Q}=2\pi(0,0,1)$ for concreteness, and the upper and lower signs refer to the A and B sublattices, respectively. The parameters n, q, t_α, and t_β are positive at all $T>0$ in the AFM phase. However, note that n vanishes in the limit $T\to 0$, in agreement with the vanishing dipole moment discussed earlier for the AFM ground state.

In the FM110 state, the nonzero expectation values are

$$\langle \boldsymbol{j}_i \rangle = m(1,1,0) \pm n(1,-1,0), \tag{73}$$

$$\langle Q_i^{3z^2} \rangle = q, \tag{74}$$

$$\langle Q_i^{x^2-y^2} \rangle = \mp q', \tag{75}$$

$$\langle \boldsymbol{T}_{i,\alpha} \rangle = t_\alpha(1,1,0) \pm \tilde{t}_\alpha(1,-1,0), \tag{76}$$

$$\langle \boldsymbol{T}_{i,\beta} \rangle = t_\beta(1,-1,0) \pm \tilde{t}_\beta(1,1,0), \tag{77}$$

where again we took $\boldsymbol{Q}=2\pi(0,0,1)$ and the upper/lower signs refer to the A/B sublattices. In this case the parameters $m,n,q,q',t_\alpha,\tilde{t}_\alpha,t_\beta,\tilde{t}_\beta$ are all nonzero at temperatures within the FM110 phase including $T=0$.

The third-ordered phase dominating the phase diagram is the quadrupolar one (For the purposes of this section, we ignore the FM100 phase, which extends into a narrow region of ferromagnetic state with variable polarization direction at $T>0$, as it occupies a very small volume of the phase diagram). In the quadrupolar state, there is only a single nonvanishing order parameter,

$$\langle Q_i^{x^2-y^2} \rangle = \mp q'. \tag{78}$$

Let us discuss the symmetries of these three states. In the AFM and FM110 phases, time-reversal symmetry is broken. However, the net magnetization vanishes in the AFM state. In the AFM state, this is guaranteed by invariance under the combined operations of translation [such as by (0,1/2,1/2), which interchanges the A and B sublattices] and time reversal. No such symmetry can be combined with time reversal in the FM110 case. Various point-group symmetries are also present in the AFM and FM110 phases but we do not describe this in detail.

In the quadrupolar case, time-reversal symmetry is unbroken, which is sufficient to require the dipolar and octupolar order parameters to vanish. Only point-group symmetries are broken by the quadrupolar order. Fourfold (C_4) rotations about the x or y axes, and threefold (C_3) rotations about [111] axes are broken in this state. While the C_4 rotation about the z axis is also broken, the combination of this C_4 rotation and a translation exchanging the A and B sublattices remains a symmetry of the quadrupolar state.

A standard classification scheme for quadrupolar states is to examine the examine the eigenvalues of the $Q_i^{\mu\nu}$ matrix. These must sum to zero because the matrix is traceless. States in which there are only two distinct eigenvalues, i.e., eigs$(Q)=\{q,q,-2q\}$ are called *nematics*, and correspond to the situation in which one principal axis is distinguished from the other two, which remain identical. In the most general case, there are three distinct eigenvalues, i.e., eigs$(Q)=\{q_1,q_2,-q_1-q_2\}$, with $q_1\neq q_2$. This is called a *biaxial nematic* and is a state in which all three principal axes are distinct. The quadrupolar state obtained here is such a biaxial nematic. Physically, the local susceptibility in this state takes distinct values $\chi^{xx}_{\text{local}},\chi^{yy}_{\text{local}},\chi^{zz}_{\text{local}}$ for fields along each of the axes. However, note from Eq. (78) that the quadrupolar order parameter changes sign between the two sublattices. Thus we should properly call this state an *antiferrobiaxial nematic*. Due to the staggered ordering, the bulk susceptibility does not distinguish all three axes. Instead, there are only two distinct components, $\chi^{xx}=\chi^{yy}\neq\chi^{zz}$. The difference between the two components of the susceptibility serves as a simple macroscopic means to observe quadrupolar ordering.

C. Cubic system: Phase diagram and transitions

By solving the mean-field equations numerically, we have determined the phase diagram for the cubic case. Parts of it can be understood analytically. Suppose that the transitions from the high-temperature normal phase to the quadrupolar and AFM phases are second order. This appears to be always true for the quadrupolar phase, while it true for the AFM for most parameters, but weakly violated in some regions. With this assumption, we can determine the critical temperatures for these transitions by the usual condition of marginal stability (vanishing of the quadratic term in the Landau theory) of the free energy. We find that the critical temperature for the quadrupolar state is

$$T_c^{\text{quad}} = \frac{43V+18J'-3J}{18} \tag{79}$$

and that for the AFM state is

$$T_c^{\text{AFM}} = \frac{J+10J'+\sqrt{73J^2+164JJ'+100(J')^2}}{36}. \tag{80}$$

Without the assumption that the transitions are continuous, the critical temperature could be higher. Thus Eqs. (79) and

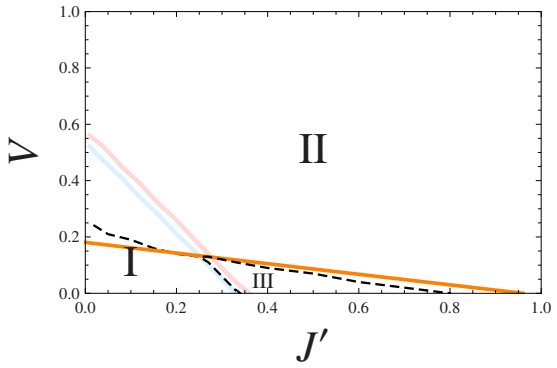

FIG. 6. (Color online) Zero-temperature two-dimensional phase diagram in the cubic case (same as Fig. 1), overlaid with the regions of different $T>0$ behavior. Dashed lines are obtained from mean-field numerics. The solid line (in orange) is defined by Eq. (81). In region I, there is a single transition to the AFM state. In region II, the system supports an intermediate-temperature quadrupolar ordered phase. The transition from the normal state to the quadrupolar phase is second order. In this region, there is a first-order transition to the AFM phase on further cooling, for parameters such that the latter is the ground state. Otherwise, the lower temperature transition is to a ferromagnetic (predominantly FM110) state. In region III, the system first turns from normal phase to the AFM state then to a ferromagnetic (predominantly FM110) state on further cooling.

(80) give lower bounds for the transition temperatures, strictly speaking. Extending the two-dimensional $T=0$ phase diagram in Fig. 1 into a third dimension of temperature, the quadrupolar phase occurs "above" the portion for which $T_c^{\mathrm{quad}} > T_c^{\mathrm{AFM}}$, which implies $V > V_c$, with

$$V_c = \frac{7J - 26J' + \sqrt{73J^2 + 164JJ' + 100(J')^2}}{86}. \qquad (81)$$

The curve $V_c(J')$ defines an almost straight line in the 2D phase diagram, as shown in Fig. 6. In fact, Eq. (81) slightly underestimates V_c, as it assumes the normal to AFM transition is continuous, when it is in fact weakly first order in this vicinity. However, the true V_c found numerically is only a few percent larger. For $V < V_c$, no quadrupolar phase occurs. Instead, the first ordering transition from high temperature is into the AFM state. This is true even when the ground state is ferromagnetic, so that in this case (when $V < V_c$) the system first orders into the AFM state, and then at lower temperature switches to the FM110 phase.

We now discuss the nature of the transitions. The quadrupolar ordering transition is, as already mentioned, continuous (see Figs. 7 and 8). It is described by a single scalar order parameter [equal to q' in Eq. (78)], for each of the three [100] wave vectors, describing the associated staggered quadrupole moment. Formally,

$$\phi_a = (-1)^{2x_i^a} \langle Q_i^{x^2-y^2} \rangle, \qquad (82)$$

where $x_i^1 = x_i$, $x_i^2 = y_i$, $x_i^3 = z_i$. According to symmetry, the Landau free energy for ϕ_a has the same form as that for an O(3) magnetic transition with cubic anisotropy. Beyond mean-field theory, this is believed to support a three-dimensional transition in the O(3) universality class.

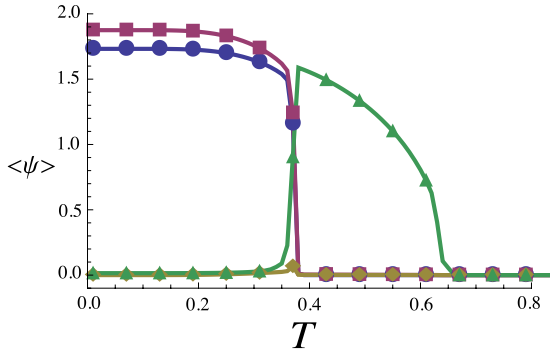

FIG. 7. (Color online) Temperature dependence of order parameters for $J'/J=0.1$ and $V/J=0.3$. For these parameters, there is a continuous normal to quadrupolar transition, at $T/J \approx 0.65$, followed by a first-order transition to the AFM state at $T/J \approx 0.37$. The four order parameters plotted are: squares (red) $|\langle \boldsymbol{T}_{A,\alpha} - \boldsymbol{T}_{B,\alpha} \rangle|/2$, circles (blue) $\langle Q_A^{3z^2} + Q_B^{3z^2} \rangle/2$, diamonds (yellow) $|\langle \boldsymbol{j}_A - \boldsymbol{j}_B \rangle|/2$, and triangles (green) $\langle Q_A^{x^2-y^2} - Q_B^{x^2-y^2} \rangle/2$. In the figure, $J=1$.

The transition from the normal to the AFM state is continuous in mean-field theory for small V (see Fig. 9), becoming weakly first order for larger V, close to V_c where the intermediate quadrupolar phase emerges. The normal-AFM transition is characterized, for each of the three wave vectors, by a two-component primary order parameter, which could be taken to be the two components of $\boldsymbol{T}_{A,\alpha}$ normal to $\boldsymbol{Q}$. In principle, the degeneracy of the ordering pattern within this "XY" plane normal to $\boldsymbol{Q}$ is, as we have remarked, accidental, and should be removed by additional effects. We do not, however, observe this degeneracy lifting within mean-field theory for the present model. With the degeneracy, the transition should be therefore described by the free energy for some six-component order parameter. As we do not understand the degeneracy lifting mechanism at present, we do not attempt here to establish the true critical properties for this transition (when it is continuous) with fluctuations taken into account.

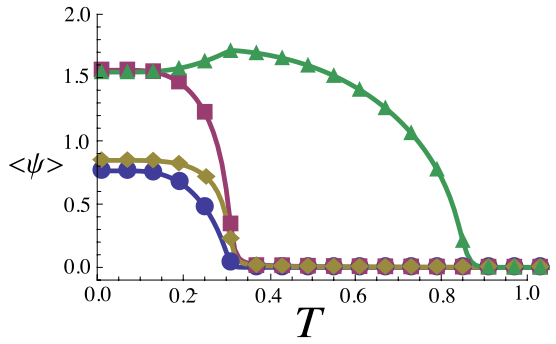

FIG. 8. (Color online) Temperature dependence of order parameters for $J'/J=0.3$ and $V/J=0.3$. For these parameters, there is a continuous normal to quadrupolar transition, at $T/J \approx 0.85$, followed by a continuous quadrupolar to FM110 transition at $T/J \approx 0.33$. The four order parameters plotted are: squares (red) $|\langle \boldsymbol{T}_{A,\alpha} - \boldsymbol{T}_{B,\alpha} \rangle|/2$, circles (blue) $\langle Q_A^{3z^2} + Q_B^{3z^2} \rangle/2$, diamonds (yellow) $|\langle \boldsymbol{j}_A + \boldsymbol{j}_B \rangle|/2$, and triangles (green) $\langle Q_A^{x^2-y^2} - Q_B^{x^2-y^2} \rangle/2$. In the figure, $J=1$.

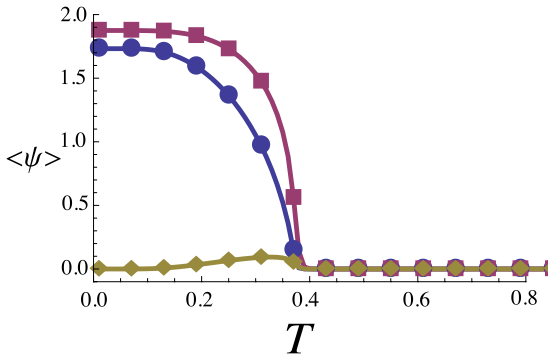

FIG. 9. (Color online) Temperature dependence of order parameters for $J'/J=0.2$ and $V/J=0.1$. For these parameters, there is a direct, continuous, normal to AFM transition, at $T/J\approx 0.38$. The three curves show: squares (red) $|\langle \boldsymbol{T}_{A,\alpha}-\boldsymbol{T}_{B,\alpha}\rangle|/2$, circles (blue) $\langle Q_A^{3z^2}+Q_B^{3z^2}\rangle/2$, and diamonds (yellow) $|\langle \boldsymbol{j}_A-\boldsymbol{j}_B\rangle|/2$. Note: in this figure and in Figs. 7, 8, and 10, the symbols are not the data points (which are much more dense)—they simply label the different curves. In the figure, $J=1$.

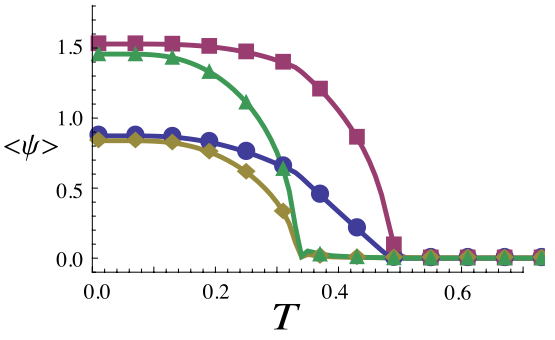

FIG. 10. (Color online) Temperature dependence of order parameters for $J'/J=0.40$ and $V/J=0.05$. For these parameters, there is a continuous normal to AFM transition, at $T/J\approx 0.49$, followed by a continuous AFM to FM110 transition at $T/J\approx 0.34$. The four order parameters plotted are: squares (red) $|\langle \boldsymbol{T}_{A,\alpha}-\boldsymbol{T}_{B,\alpha}\rangle|/2$, circles (blue) $\langle Q_A^{3z^2}+Q_B^{3z^2}\rangle/2$, diamonds (yellow) $|\langle \boldsymbol{j}_A+\boldsymbol{j}_B\rangle|/2$, and triangles (green) $\langle Q_A^{x^2-y^2}-Q_B^{x^2-y^2}\rangle/2$. In the figure, $J=1$.

The quadrupolar to FM110 transition is continuous in mean-field theory (see Fig. 8). This could be anticipated by examining the form of the order parameters in the FM110 phase. We note that the antiferrobiaxial nematic order parameter of the quadrupolar state is already nonvanishing in the FM110 phase. Hence, we might naturally expect, upon heating, that thermal fluctuations first restore time-reversal symmetry, yielding the quadrupolar phase, before fully restoring all symmetry in the normal state. To determine the nature of the order parameter for this transition, note that the wave vector and local anisotropy axes are already established in the quadrupolar state. Hence the direction of the uniform and staggered magnetizations are already determined, up to a sign and interchange, above the transition. For instance, for the quadrupolar state in Eq. (78), with $\boldsymbol{Q}=2\pi(001)$, the uniform magnetization can lie along $\pm(110)$ and the staggered magnetization along $\pm(1\bar{1}0)$, or vice versa. Thus the symmetry breaking from the quadrupolar to the FM110 state is described by two Ising order parameters. We therefore expect this transition, beyond mean-field theory, to be similar to that of an Ashkin-Teller or similar models.

The quadrupolar to AFM transition appears strongly first order (see Fig. 7). This is in agreement with the expectations of Landau theory, as the symmetry of the AFM phase is not a subgroup of the symmetry of the quadrupolar one. In terms of order parameters, this is evident since $\langle Q_i^{x^2-y^2}\rangle$ is nonzero in the quadrupolar phase but zero in the AFM one, while the magnetic order parameters are zero in the quadrupolar phase but nonzero in the AFM. Fine tuning of the free energy would be required to arrange both these types of order to change at the same temperature in a continuous fashion.

In region III one encounters a transition from the AFM to FM110 state. This appears to be continuous in mean-field theory (see Fig. 10). One can understand this by noting that the AFM solution can be regarded as a subset of the FM110 one, if the unit vector $(u_1,u_2,0)$ is taken to be along $(1,-1,0)$. Then the transition to the FM110 is described by the emergence of a nonzero m. Like the normal to AFM transition, because we have not understood the degeneracy-breaking mechanism in the AFM state, we do not attempt to analyze this transition beyond MFT.

D. Effects of anisotropy

We now consider the effects of anisotropy on the $T>0$ phase diagram, focusing on the case of weak $|D|\ll J,J',V$. We have already considered the effects of D on the AFM and FM110 states in Sec. III B 4. We saw that easy-axis anisotropy favors states with the wave vector $\boldsymbol{Q}$ parallel to the z (easy) axis. This is because the anisotropy couples directly to the $Q_i^{3z^2}$ field,

$$H_D=-D\sum_i (j_i^z)^2=\text{const}-\frac{D}{\sqrt{3}}\sum_i Q_i^{3z^2}. \tag{83}$$

Both the AFM and FM110 states have a nonzero and constant expectation value of $Q_i^{3z^2}$, which is maximized in this orientation. Conversely, easy-plane anisotropy favors states with the wave vector $\boldsymbol{Q}$ perpendicular to the z (hard) axis, for the same reason.

We now repeat this analysis for the quadrupolar state. Here the situation is more subtle because $\langle Q_i^{3z^2}\rangle$ vanishes in the quadrupolar state. Moreover, the cubic rotations (e.g., $\langle Q_i^{3x^2}\rangle$), while not vanishing, give zero net contribution due to the opposite signs on the A and B sublattices. This means that the splitting of the different wave-vector states vanishes at linear order in D. There is instead a quadratic contribution, which, numerically, we find favors the states with $\boldsymbol{Q}$ parallel to z (see Fig. 11). Being quadratic in D, this same configuration is favored *for both the easy-axis and easy-plane cases*. Thus we have the interesting situation that for easy-plane anisotropy, the wave vector orients parallel to z in the quadrupolar phase, but perpendicular to z in the low-temperature phase. Note that the quadrupolar phase remains distinct from the normal phase even with nonzero D, as it continues to break symmetries, notably translational invariance.

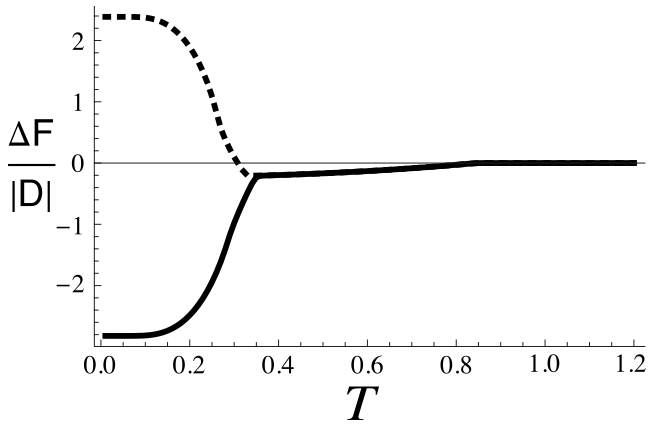

FIG. 11. Temperature dependence of the free-energy difference between states with wave vector parallel and perpendicular to the Ising axis, in the presence of a weak anisotropy $|D|=0.05$. Here $J'/J=V/J=0.3$. Solid line: $\Delta F=F(\boldsymbol{Q}\|\hat{z};D=0.05)-F(\boldsymbol{Q}\perp\hat{z};D=0.05)$. Dotted line: $\Delta F=F(\boldsymbol{Q}\|\hat{z};D=-0.05)-F(\boldsymbol{Q}\perp\hat{z};D=-0.05)$. One sees that in the quadrupolar phase, both signs of anisotropy favor the wave vector aligned with the z axis. In the FM110 phase, however, this is favored only for $D>0$. For $D<0$ (easy-plane anisotropy), the state with wave vector normal to z is preferred. Note also that the energy difference is much larger in the FM110, consistent with the expected linear and quadratic dependence on D in FM110 and quadrupolar phases, respectively. In the figure, $J=1$.

E. Magnetic susceptibility

In this section, we discuss the magnetic response at $T>0$, which is an important indicator, especially of the quadrupolar ordering transition. At high temperature, of course, one observes Curie-Weiss behavior. For the general Hamiltonian with anisotropy D, there are two different Curie-Weiss temperatures, for fields parallel and perpendicular to z,

$$\Theta_{\mathrm{CW}}^{zz}=-\frac{J}{5}+\frac{32J'}{45}+\frac{4D}{5},$$

$$\Theta_{\mathrm{CW}}^{xx}=-\frac{J}{5}+\frac{32J'}{45}-\frac{2D}{5}. \tag{84}$$

These are obtained from the high-temperature expansion of the susceptibility up to $O(1/T^2)$. These expressions may be useful in extracting exchange constants from experiment. Interestingly, if one calculates the powder average susceptibility, the contributions of the anisotropy cancel at this order and the Curie-Weiss temperature measured in this way is independent of D. It is also interesting to note that, in the region of larger V/J and small J'/J, one obtains a ferromagnetic ground state with an antiferromagnetic (negative) Curie-Weiss temperature.

On lowering temperature, the susceptibility shows distinct behaviors in the different parts of the phase diagram. We focus here for simplicity on the cubic system, starting with region I. Here the susceptibility displays the usual cusp associated with antiferromagnetic order, at the normal to AFM transition. The inverse susceptibility is plotted in Fig. 12 for $J'=V=0.1J$, in the midst of region I. It shows a minimum at the transition, and pronounced curvature below the transition

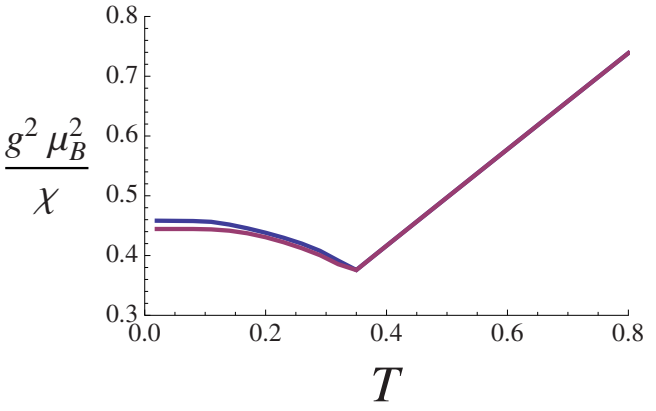

FIG. 12. (Color online) Inverse susceptibility at the normal to AFM transition for $J'=V=0.1J$. Blue (upper) curve: $1/\chi_{xx}$ and red (lower) curve: $1/\chi_{zz}$. In the figure, $J=1$.

temperature, saturating to a large constant value in the $T\to 0$ limit. We note that the large zero-temperature susceptibility is not related to gapless excitations, but is a general consequence of strong SOC, and should be expected in all parameter regimes of this model.

Next consider region II. Here, one observes a cusp at the normal to quadrupolar transition. This cusp is, however, rather different from the one just mentioned. Specifically, it is not a minimum of $1/\chi$, and instead separates two distinct "Curie-Weiss" regimes in which $1/\chi$ is linear but with different, positive, slopes (i.e., different effective magnetic moments). The presence of a lower temperature Curie-Weiss regime is a signature of quadrupolar order. This is because the quadrupolar mean field splits only the point-group degeneracy of the spins, but preserves a local Kramer's doublet. This doublet gives rise to a Curie law. An example is plotted in Fig. 13. As the quadrupolar order lowers the symmetry of the system to tetragonal, we see actually two different effective moments in susceptibility parallel to the wave vector $\boldsymbol{Q}$ (χ_{zz}) and perpendicular to it ($\chi_{xx}=\chi_{yy}$). We observe that the effective magnetic moment seen in χ_{xx} is typically *enhanced* in the quadrupolar phase, while it is suppressed in χ_{zz}, both

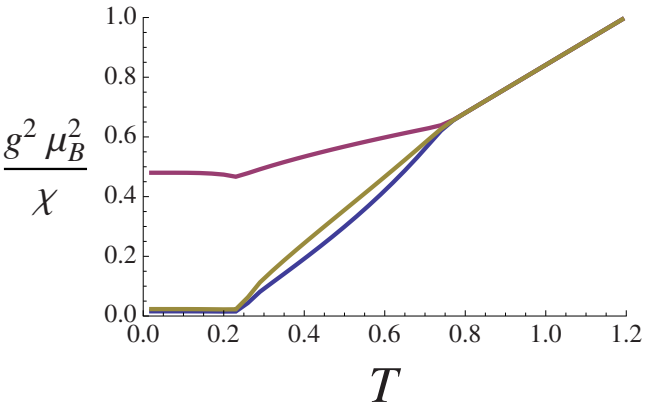

FIG. 13. (Color online) Inverse susceptibility for $J'=0.2J$ and $V=0.3J$. Blue (lower) curve: $1/\chi_{xx}$, red (upper) curve: $1/\chi_{zz}$, and yellow (middle) curve: $1/\chi_{\mathrm{powder}}$. For these parameters the quadrupolar transition is at $T/J\approx 0.75$, and the ferromagnetic transition is at $T/J\approx 0.23$. In the figure, $J=1$.

relative to the isotropic effective magnetic moment in the normal phase.

At still lower temperature, one encounters the ferromagnetic phases. Here of course the susceptibility for the easy directions diverges. Focusing on the dominant FM110 phase, one sees that since the easy direction is in the (001) plane selected by the quadrupolar order, χ_{zz} does not diverge, but χ_{xx} and χ_{yy} do.

V. BEYOND MEAN FIELD: SPIN WAVES AND NONMAGNETIC GROUND STATES

In Sec. V A, we obtained the mean-field phase diagram. Here we consider quantum effects beyond mean field. We first consider spin-wave fluctuations and obtain the collective mode spectrum in linear spin-wave theory. From this, we obtain the quantum correction to the order parameter, and, in the ideal case of $J'=V=0$, we will see that this is very large and invalidates the mean-field theory in the vicinity of this parameter regime. This suggests the possibility of very different states dominated by quantum fluctuations. We then explore this possibility, considering some candidate nonmagnetic ground states of our model.

First, we consider the quantum ground states of pairs of sites, unveiling a pseudosinglet structure, analogous to the $S=0$ singlet ground states for pairs of antiferromagnetically interacting spins with SU(2) symmetry. This leads naturally to the possibility of "valence-bond" states built from these pseudosinglets. We consider both a static, VBS state, and states in which the valence bonds are fluctuating, in which case we obtain a QSL state.

Very little theoretical work has been done on QSL states in systems with strong spin-orbit coupling, i.e., with strongly broken SU(2) symmetry. As such, the structure of possible QSL states in the present model requires particular investigation. Guided by the pseudosinglet structure, and the hidden SU(2) symmetry of the model, we construct candidate QSL states for the full Hamiltonian, $\tilde{\mathcal{H}}_{\text{ex-1}}$, by a slave-particle technique.

A. Spin waves

In the previous two sections, we have discussed the state phase diagram based on mean-field theory. Here, we perform a linear spin-wave analysis, which perturbatively describes the effect of quantum fluctuations on the various phases obtained so far, and also predicts the structure of collective modes, which might, e.g., be observed in inelastic neutron scattering. Finally, because we have not explored the full space of mean-field states, the calculation also provides an important check that the phases we have found are at least metastable.

The conventional Holstein-Primakoff (HP) transformation for spin-S operators cannot be directly applied for the three variational ground states because none of the three states is a fully polarized state for any projection of the spin angular momentum operator $\boldsymbol{j}$. This is especially severe for the AFM state, for which the spin expectation value simply vanishes. Instead, we formulate an "SU(4) spin-wave theory," by rewriting the Hamiltonian, Eq. (27), in a bilinear form in terms of the 15 generators of the SU(4) group. To do so, we introduce, for any local basis for the single-site Hilbert space $\{|n\rangle\}, n=1,2,3,4$, the complete set of operators[40]

$$\mathcal{S}_m^n = |m\rangle\langle n|. \tag{85}$$

These SU(4) generators obey the algebra $[\mathcal{S}_m^n, \mathcal{S}_k^l] = \delta_{nk}\mathcal{S}_m^l - \delta_{ml}\mathcal{S}_k^n$. We can then use the HP transformation for the generators of SU(4). In this transformation, one selects a particular state in the four-dimensional basis to be the vacuum and introduces three bosons associated with excitations to the three other states. For the AFM phase, the classical ground state is given by Eq. (40). Hence we take, on the A sublattice (z_i integer), the basis

$$|1\rangle_A = \frac{1}{\sqrt{2}}(|3/2\rangle + e^{i\phi}|-3/2\rangle), \quad |2\rangle_A = |1/2\rangle,$$

$$|3\rangle_A = |-1/2\rangle, \quad |4\rangle_A = \frac{1}{\sqrt{2}}(|3/2\rangle - e^{i\phi}|-3/2\rangle), \tag{86}$$

while for sublattice B (z_i half integer),

$$|1\rangle_B = \frac{1}{\sqrt{2}}(|3/2\rangle - e^{i\phi}|-3/2\rangle), \quad |2\rangle_B = |-1/2\rangle,$$

$$|3\rangle_B = |1/2\rangle, \quad |4\rangle_B = \frac{1}{\sqrt{2}}(|3/2\rangle + e^{i\phi}|-3/2\rangle). \tag{87}$$

The Hamiltonian $\tilde{\mathcal{H}}$ in Eq. (27) in this basis has a quadratic form,

$$\tilde{\mathcal{H}} = \sum_{\langle ij\rangle} C_{klmn}(i,j)\mathcal{S}_k^l(i)\mathcal{S}_m^n(j), \tag{88}$$

where the coefficients $C_{klmn}(i,j)$ (which are straightforward to obtain, so we do not give them explicitly) depend linearly on J, J', and V.

To introduce the HP transformation on sublattice A (B), we choose $|1\rangle$ as the vacuum which is annihilated by three "magnon" annihilation operators a_n (b_n), $n=2,3,4$. One can think these three bosons as descending from mixed spin and orbitals fluctuations of the Hamiltonian before the $\mathcal{P}_{3/2}$ projection. The HP transformation is defined as,[41] for i in the A sublattice,

$$\mathcal{S}_1^1(i) = M - \sum_{n\neq 1} a_n^\dagger(i)a_n(i), \tag{89}$$

$$\mathcal{S}_n^1(i) = a_n^\dagger(i)\sqrt{M - \sum_{l\neq 1} a_l^\dagger(i)a_l(i)} \quad (n\neq 1), \tag{90}$$

$$\mathcal{S}_n^l(i) = a_n^\dagger(i)a_l(i) \quad (l,n\neq 1), \tag{91}$$

while for i in the B sublattice, the same formula holds with $a_n(i)$ replaced by $b_n(i)$. In the above equations M is defined as the number of columns in the Young tableaux for the representation of SU(4). In our case (fundamental representation), we must set $M=1$. In the generalization to arbitrary M, the classical limit where the classical ground state be-

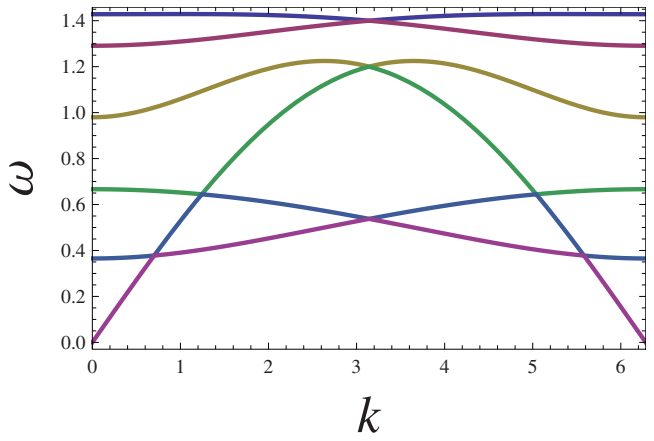

FIG. 14. (Color online) Spin-wave spectrum for the AFM phase at $J'=0.1$ and $V=0.2$ along [001] momentum direction and $J=1$. There is one low-lying gapless mode. The fcc lattice constant is set to be $a=1$ and the phase $\phi=0$ for the ground state in Eq. (40).

comes exact is $M\to\infty$. However, we apply this HP transformation directly for $M=1$. Inserting this into Eq. (88), we expand it to obtain a quadratic form in the bosonic operators. The constant term in the expansion gives the classical ground-state energy,

$$\frac{E_{\mathrm{AFM}}}{\mathcal{N}} = M^2\left(-\frac{J}{2}+J'+\frac{11V}{12}\right), \tag{92}$$

independent of the phase ϕ. The quadratic terms lead to quantum corrections. Defining the Fourier transform of the bosonic operators, the spin-wave Hamiltonian can be organized in the form $\Sigma_{\mathbf{k}}H_{\mathbf{k}}$ with

$$H_{\mathbf{k}} = (\mathcal{A}_{\mathbf{k}}^{\dagger} \quad \mathcal{A}_{-\mathbf{k}}) \begin{pmatrix} F_{\mathbf{k}} & G_{\mathbf{k}}^{\dagger} \\ G_{\mathbf{k}} & F_{\mathbf{k}} \end{pmatrix} \begin{pmatrix} \mathcal{A}_{\mathbf{k}} \\ \mathcal{A}_{-\mathbf{k}}^{\dagger} \end{pmatrix}, \tag{93}$$

where $\mathcal{A}_{\mathbf{k}}=(a_{2\mathbf{k}},a_{3\mathbf{k}},a_{4\mathbf{k}},b_{2\mathbf{k}},b_{3\mathbf{k}},b_{4\mathbf{k}})$ is the vector of magnon annihilation operators and $F_{\mathbf{k}}$ and $G_{\mathbf{k}}$ are 6×6 matrices. This spin-wave Hamiltonian can be diagonalized by standard methods.[42]

For the AFM ground state, Eq. (40), we obtain a gapless magnon mode, as depicted in Fig. 14. This gapless mode is associated with the continuous accidental degeneracy and indeed occurs for arbitrary ϕ. By contrast, in the FM110 and FM100 phases, one observes a gap for all the spin wave modes (see Figs. 15 and 16). The gap in the FM110 phase increases with J', as expected since this corresponds to increasingly violated SU(2) symmetry. In all cases, the modes are all well defined with positive real frequencies, indicating the stability of the phases in the classical sense: i.e., that we have properly found local energy minima of the mean-field theory.

Finally, having obtained the spin-wave modes, we can evaluate the quantum corrections. It is most interesting to consider the reduction in the order parameter by quantum fluctuations. We can define this by considering the probability to find a given spin in its mean-field ground state. This is nothing but the vacuum state of the HP bosons. Hence this probability is given, for a site on the A sublattice, by

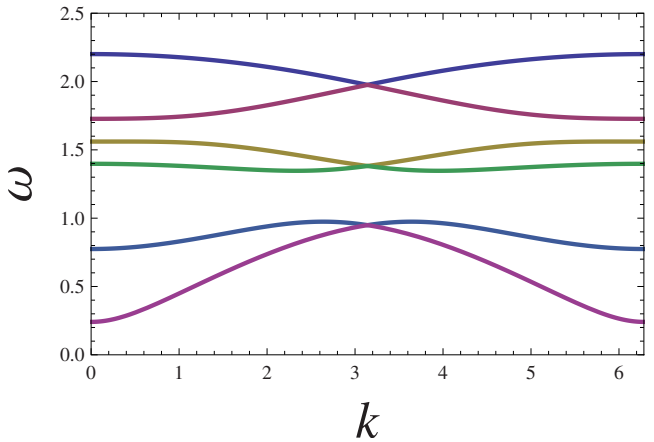

FIG. 15. (Color online) Spin-wave spectrum for the FM110 phase at $J'=0.3$ and $V=0.2$ along [001] momentum direction. The lowest excitation mode has an energy gap $\Delta=0.241$ at $k=0$. In the graph, $J=1$.

$$P_{gs}(i) = \langle 1 - \sum_{n\neq 1} a_n^{\dagger}(i)a_n(i)\rangle. \tag{94}$$

This quantity is directly analogous to the staggered magnetization in the usual HP treatment of a quantum antiferromagnet. We therefore denote $\Delta M=1-P_{gs}(i)=\Sigma_{n\neq 1}\langle a_n^{\dagger}(i)a_n(i)\rangle$. This is obtained, at $T=0$, by integrating the zero-point contribution to the boson number from each spin-wave mode. The quadratic spin-wave Hamiltonian is diagonalized by a Bogoliubov transformation $\mathcal{Q}_{\mathbf{k}}$,

$$(\mathcal{C}_{\mathbf{k}},\mathcal{C}_{-\mathbf{k}}^{\dagger})^T = \mathcal{Q}_{\mathbf{k}}(\mathcal{A}_{\mathbf{k}},\mathcal{A}_{-\mathbf{k}}^{\dagger})^T, \tag{95}$$

in which, $\mathcal{C}_{\mathbf{k}}=(c_{1\mathbf{k}},c_{2\mathbf{k}},c_{3\mathbf{k}},c_{4\mathbf{k}},c_{5\mathbf{k}},c_{6\mathbf{k}})$, and $\mathcal{Q}_{\mathbf{k}}$ is a 12×12 matrix. From this we obtain the quantum correction

$$\Delta M = \frac{1}{\mathcal{N}}\sum_{n\neq 1}\Big[\sum_{i\in A} a_n^{\dagger}(i)a_n(i) + \sum_{i\in B} b_n^{\dagger}(i)b_n(i)\Big] = \frac{1}{2}\left\{\frac{1}{\mathcal{N}}\sum_{\mathbf{k}}\sum_{i=1}^{6}[\mathcal{Q}^{\dagger}\mathcal{Q}]_{ii} - 3\right\}. \tag{96}$$

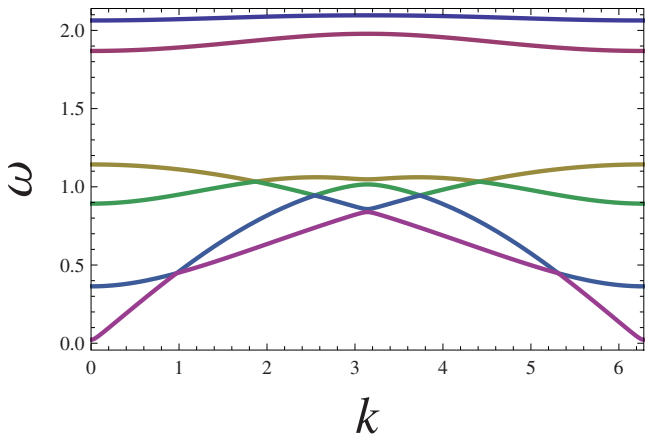

FIG. 16. (Color online) Spin-wave spectrum for the FM100 phase at $J'=0.1$ and $V=0.4$ along [001] momentum direction. The lowest excitation mode has an energy gap $\Delta=0.0224$ at $k=0$. In the graph, $J=1$.

Numerically, we find that this quantum correction is maximal for $J'=V=0$, and is given by $\Delta M \approx 1.7$ at this point. This is much larger than 1, implying that the fluctuations at this point are large and that the mean-field theory is at least quantitatively invalid. For increasing J' and V the correction becomes significantly smaller and mean-field theory may be reliable. In the vicinity of the $J'=V=0$, one may expect a very different ground state, incorporating strong quantum fluctuations. We explore some possible *nonmagnetic* ground states in the remainder of this section.

B. Pseudosinglets in different planes

We start our analysis of nonmagnetic states by considering two sites in the XY plane, which interact with the Hamiltonian $\tilde{\mathcal{H}}^{\mathrm{XY}}_{\mathrm{ex-1}}(i,j)$. Remarkably, the ground state has a form identical to an SU(2) spin singlet, if written in terms of pseudospin-1/2 states $j^z=\pm 1/2$,

$$|\mathrm{XY}\rangle_{ij} = \frac{1}{\sqrt{2}}\left(\left|\frac{1}{2}\right\rangle_i\left|-\frac{1}{2}\right\rangle_j - \left|-\frac{1}{2}\right\rangle_i\left|\frac{1}{2}\right\rangle_j\right). \tag{97}$$

One may understand this result by writing down the projected spin and occupation number operators in xy orbitals, in the basis of j^z eigenstates [see Eq. (23)],

$$\tilde{\boldsymbol{S}}_{xy} = \frac{1}{3}\begin{pmatrix} 0 & & \\ & \boldsymbol{\sigma} & \\ & & 0 \end{pmatrix}, \tag{98}$$

$$\tilde{n}_{xy} = \frac{2}{3}\begin{pmatrix} 0 & & \\ & I_2 & \\ & & 0 \end{pmatrix}. \tag{99}$$

Here $\boldsymbol{\sigma}$ is the vector of Pauli matrices and I_2 is the 2×2 identity matrix. One may consider $\tilde{\boldsymbol{S}}_{xy}$ as an effective spin-1/2 operator in the subspace of $j^z=\pm 1/2$ states, which naturally explains the SU(2) singlet in Eq. (97).

For the XZ and YZ planes, one simply needs to apply a cubic permutation to the results obtained for XY planes, or more formally, apply a unitary transformation that rotates about the [111] axis by $\pm 2\pi/3$,

$$\tilde{S}^{\mu'}_{xz} = U^\dagger \tilde{S}^{\mu}_{xy} U, \tag{100}$$

$$\tilde{S}^{\mu''}_{yz} = U \tilde{S}^{\mu}_{xy} U^\dagger \tag{101}$$

with

$$U = \exp\left(-i\frac{2\pi}{3}\frac{j^x+j^y+j^z}{\sqrt{3}}\right). \tag{102}$$

The upper indices $\mu'=p(\mu)$ and $\mu''=p^{-1}(\mu)$ in Eqs. (100) and (101) denote cyclic and anticyclic permutations of x,y,z, respectively [i.e., $p:(x,y,z)\to(y,z,x)$ with inverse $p^{-1}:(x,y,z)\to(z,x,y)$]. The two-site ground states in the XZ and YZ planes are the pseudosinglets in the subspace of $j^y=\pm 1/2$ states and $j^x=\pm 1/2$ states, respectively.

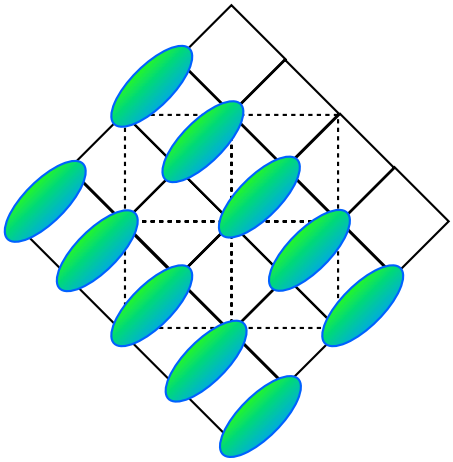

FIG. 17. (Color online) Columnar valence-bond solid (VBS) state within an XY plane. The dashed square indicates the face of a conventional cubic unit cell, while the solid lines connect the fcc nearest neighbors within the plane, which form a 45° rotated square lattice.

C. Valence-bond solid state

It is natural to consider a product state of such pseudosinglet "valence bonds" (also called "dimers") as a candidate (prototypical variational) nonmagnetic ground state. To do so, we must divide the spins into two neighboring sublattices, which will be paired. This by necessity breaks lattice symmetries. Such a state is called a valence-bond solid, or VBS, state. At the level of valence-bond product states, many possible arrangements of the dimers are degenerate. This degeneracy is artificial and will be broken if the wave functions are improved. We will not investigate this in any detail and just consider the simplest VBS state in which the dimers form a "columnar" arrangement within a single (001) plane, see Fig. 17.

The variational energy of such a state (actually any state with a planar arrangement of dimers has the same energy) is readily evaluated. We obtain the energy per site $E_{\mathrm{VBS}}/\mathcal{N} = \langle \mathrm{VBS}|\tilde{H}_{ex-1}|\mathrm{VBS}\rangle/\mathcal{N} = -5/12J = -0.42J$. This is slightly higher than the mean-field ground-state energy of the AFM state, $E^{\mathrm{MF}}_{\mathrm{AFM}}/\mathcal{N} = -J/2$. However, the large quantum fluctuations are expected to destabilize the latter state and perhaps might stabilize the VBS one. So such a VBS state seems competitive and may be considered as a possibility for future exploration.

D. QSLs and fermionic mean-field theory

The most general approach that has been applied to describe QSL states is the slave-particle method, in which auxiliary fermions are introduced, and the ground state for the spin system is described by some projection of a nominally simple fermionic state into the physical spin Hilbert space. This results, in the usual SU(2)-invariant case, in wave functions which are composed of superpositions of products of SU(2) singlets. Here, the appearance of two-site pseudosinglet ground states points to the possibility of applying a similar fermionic mean-field theory. In this section, we

implement this technique for the full antiferromagnetic exchange interaction.

We first introduce the auxiliary fermionic creation operators, whose quanta we call "spinons,"[40]

$$|\alpha\rangle_i = f_{i\alpha}^\dagger |\text{vacuum}\rangle, \quad \alpha = 1, \ldots 4, \tag{103}$$

where for convenience we have relabeled the states $j^z = \frac{3}{2}, \frac{1}{2}, -\frac{1}{2}, -\frac{3}{2}$ by $\alpha = 1,2,3,4$, respectively. The physical Hilbert space is constructed from states with one fermion at each site, which imposes the constraint

$$\sum_{\alpha=1}^{4} f_{i\alpha}^\dagger f_{i\alpha} = 1. \tag{104}$$

In this notation, the spin and number operators become

$$\tilde{\boldsymbol{S}}_{i,xy} \Rightarrow F_i^\dagger \tilde{\boldsymbol{S}}_{i,xy} F_i, \tag{105}$$

$$\tilde{n}_{i,xy} \Rightarrow F_i^\dagger \tilde{n}_{i,xy} F_i, \tag{106}$$

where on the right-hand side it is to be understood that the matrices in Eqs. (98) and (99) act on the vector of spinon operators

$$F_i = (f_{i1}, f_{i2}, f_{i3}, f_{i4})^{\mathrm{T}}. \tag{107}$$

Similar expressions can readily be written for operators in XZ and YZ planes. Thus the Hamiltonian in terms of spinons reads

$$\begin{aligned}\tilde{\mathcal{H}}_{\text{ex-1}}^{\text{XY}}(ij) &= J\Big[(F_i^\dagger \tilde{\boldsymbol{S}}_{i,xy} F_i) \cdot (F_j^\dagger \tilde{\boldsymbol{S}}_{j,xy} F_j) \\ &\quad - \frac{1}{4} (F_i^\dagger \tilde{n}_{i,xy} F_i) \cdot (F_j^\dagger \tilde{n}_{j,xy} F_j) \Big] \\ &= \frac{2J}{9} \sum_{\alpha,\beta=2,3} [-f_{i,\alpha}^\dagger f_{j,\alpha} f_{j,\beta}^\dagger f_{i,\beta} + f_{i,\alpha}^\dagger f_{j,\beta} f_{j,\beta}^\dagger f_{i,\alpha} \\ &\quad - f_{i,\alpha}^\dagger f_{i,\beta} \delta_{\alpha\beta}],\end{aligned} \tag{108}$$

in which, $\boldsymbol{\sigma}_{\alpha\beta} \cdot \boldsymbol{\sigma}_{\alpha'\beta'} = 2\delta_{\alpha\beta'}\delta_{\alpha'\beta} - \delta_{\alpha\beta}\delta_{\alpha'\beta'}$ has been used. Similar spinon Hamiltonians can also be written down for XZ and YZ planes. When we write down the full antiferromagnetic exchange Hamiltonian and sum over XY, YZ, and XZ planes, we find that the single-site terms, which are quadratic in spinon operators, sum up to a constant once we impose the single occupancy constraint. We are then left with the terms that are quartic in spinon operators.

We now follow the standard procedure of slave-particle mean-field theory to decouple the quartic terms in the spinon Hamiltonian and write down a mean-field ansatz. We start with the exchange Hamiltonian in the XY plane, $\tilde{\mathcal{H}}_{\text{ex-1}}^{\text{XY}}$.

We require a mean-field ansatz for the fermionic bond expectation values, $\langle f_{i\alpha}^\dagger f_{j\beta} \rangle$. Noting the structure of the two-site pseudosinglet in this plane, we choose an ansatz which reproduces a quantum ground state of this type. Specifically,

$$\chi_{ij;\alpha\beta} \equiv \langle f_{i\alpha}^\dagger f_{j\beta} \rangle = \chi_{ij} (\mathcal{I}_{xy})_{\beta\alpha}, \quad \langle ij \rangle \in \text{XY} \tag{109}$$

with

$$\mathcal{I}_{xy} = \begin{pmatrix} 0 & & \\ & I_2 & \\ & & 0 \end{pmatrix}. \tag{110}$$

Note that, by construction, this expectation value is invariant under the hidden SU(2) symmetry. The χ_{ij} on the XZ and YZ planes are determined by symmetry

$$\chi_{ij;\alpha\beta} \equiv \langle f_{i\alpha}^\dagger f_{j\beta} \rangle = \chi_{ij} (\mathcal{I}_{xz})_{\beta\alpha}, \quad \langle ij \rangle \in \text{XZ},$$

$$\chi_{ij;\alpha\beta} \equiv \langle f_{i\alpha}^\dagger f_{j\beta} \rangle = \chi_{ij} (\mathcal{I}_{yz})_{\beta\alpha}, \quad \langle ij \rangle \in \text{YZ}, \tag{111}$$

and

$$\mathcal{I}_{xz} = U^\dagger \mathcal{I}_{xy} U, \tag{112}$$

$$\mathcal{I}_{yz} = U \mathcal{I}_{xy} U^\dagger \tag{113}$$

with the unitary transformation introduced in Eq. (102).

We then arrive at the mean-field Hamiltonian

$$\begin{aligned}\mathcal{H}_{\text{MF}}^{\text{XY}} &= -\tilde{J} \sum_{\langle ij \rangle \in \text{XY}} [(\chi_{ij} F_j^\dagger \mathcal{I}_{xy} F_i + \text{H.c.}) - 2|\chi_{ij}|^2] \\ &\quad + \sum_i \Lambda_i (F_i^\dagger F_i - 1)\end{aligned} \tag{114}$$

with $\tilde{J} \equiv 2J/9$. Here Λ_i are the Lagrange multipliers related to the single-occupancy constraint in Eq. (104). $\mathcal{H}_{\text{MF}}^{\text{XZ}}$ and $\mathcal{H}_{\text{MF}}^{\text{YZ}}$ can be readily written down using Eqs. (111) and (112).

1. Uniform spin liquid

As discussed in Sec. II, the antiferromagnetic exchange Hamiltonian has a hidden global SU(2) symmetry, $[G^\mu, \tilde{\mathcal{H}}_{\text{ex-1}}] = 0$. It is easy to find that the full mean-field Hamiltonian we have here respects this hidden global SU(2) symmetry. We seek a quantum-spin-liquid ground state which does not break any symmetries of the original Hamiltonian. Translational invariance imposes $\Lambda_i = \Lambda = \text{const}$. First we consider the ansatz for a uniform spin liquid,

$$\chi_{ij} = \chi_{ji} = \chi, \tag{115}$$

for i,j nearest neighbors on the fcc lattice. This naturally respects point-group and time-reversal symmetries. The Hamiltonian in Eq. (114) is then diagonalized by Fourier transform

$$f_\alpha(\mathbf{k}) = \sum_j e^{-i\mathbf{k}\cdot\mathbf{R}_j} f_{j\alpha}. \tag{116}$$

We find

$$\mathcal{H}_{\text{MF}} = \sum_{\lambda=1,2} \sum_{\mathbf{k}} \epsilon_\lambda(\mathbf{k}) [\tilde{f}_{\lambda+}^\dagger(\mathbf{k}) \tilde{f}_{\lambda+}(\mathbf{k}) + \tilde{f}_{\lambda-}^\dagger(\mathbf{k}) \tilde{f}_{\lambda-}(\mathbf{k})] + 12\mathcal{N}\tilde{J}\chi^2, \tag{117}$$

where $\lambda = 1,2$ label doubly degenerate bands with dispersion

$$\epsilon_{1,2}(\mathbf{k}) \equiv \tilde{J}\chi\tilde{\epsilon}_{1,2}(\mathbf{k}) = -2\tilde{J}\chi[C_xC_y + C_yC_z + C_zC_x \pm \sqrt{C_x^2C_y^2 + C_y^2C_z^2 + C_z^2C_x^2 - C_xC_yC_z(C_x + C_y + C_z)}]. \tag{118}$$

Here $C_x=\cos(k_x/2)$, $C_y=\cos(k_y/2)$, and $C_z=\cos(k_z/2)$. The double degeneracy of the two bands is due to Kramer's degeneracy since $\boldsymbol{j}_i$ is a spin-3/2 operator and the Hamiltonian has time-reversal symmetry.

The ground-state wave function at the mean-field level is described by a Fermi sea of spinons,

$$|\Psi_{\mathrm{MF}}\rangle = \prod_{\lambda=1,2}\prod_{\mathbf{k}} \tilde{f}^{\dagger}_{\lambda+}(\mathbf{k})\tilde{f}^{\dagger}_{\lambda-}(\mathbf{k})|\mathrm{vacuum}\rangle, \tag{119}$$

for all $\mathbf{k}$ below the Fermi surface. The mean-field ground-state energy per site is

$$\frac{E_{\mathrm{MF}}}{\mathcal{N}\tilde{J}} = 2\chi\sum_{\lambda=1,2}\int\frac{d^3k}{(2\pi)^3}\theta[\mu-\tilde{\epsilon}_{\lambda}(\mathbf{k})]\tilde{\epsilon}_{\lambda}(\mathbf{k}) + 12\chi^2, \tag{120}$$

where the integral is over the first Brillouin zone of the fcc lattice and the dimensionless chemical potential μ is fixed by the quarter-filling condition,

$$2\sum_{\lambda=1,2}\int\frac{d^3k}{(2\pi)^3}\theta[\mu-\tilde{\epsilon}_{\lambda}(\mathbf{k})] = 1. \tag{121}$$

The wave function in Eq. (119) must be Gutzwiller projected into the physical Hilbert space with one spinon per site,

$$|\Psi\rangle = \mathcal{P}_{n_i=1}|\Psi_{\mathrm{MF}}\rangle. \tag{122}$$

Here we simply evaluate the ground-state energy at the mean-field level. Minimizing Eq. (120) with respect to the parameter χ, we find

$$\chi^* = -\frac{1}{12}\sum_{\lambda=1,2}\int\frac{d^3k}{(2\pi)^3}\theta[\mu-\tilde{\epsilon}_{\lambda}(\mathbf{k})]\tilde{\epsilon}_{\lambda}(\mathbf{k}) \tag{123}$$

and

$$\frac{E_{\mathrm{MF}}}{\mathcal{N}} = -\frac{8}{3}J(\chi^*)^2. \tag{124}$$

The spinon density is at quarter filling for $\mu\approx-1.58J$. The mean-field energy for the uniform spin-liquid state is then $E^{(0)}_{\mathrm{MF}}/\mathcal{N}\approx-0.041J$.

2. π-flux spin liquid

We now consider the ansatz for the π-flux spin-liquid state illustrated in Fig. 18. In order to preserve time-reversal symmetry, the phase of the χ_{ij} at each bond can only assume the values 0 or π. We divide the fcc lattice into four cubic lattices

$$\mathbf{r}^A_j = (0,0,0) + \mathbf{R}_j,$$

$$\mathbf{r}^B_j = (1/2,1/2,0) + \mathbf{R}_j,$$

$$\mathbf{r}^C_j = (0,1/2,1/2) + \mathbf{R}_j,$$

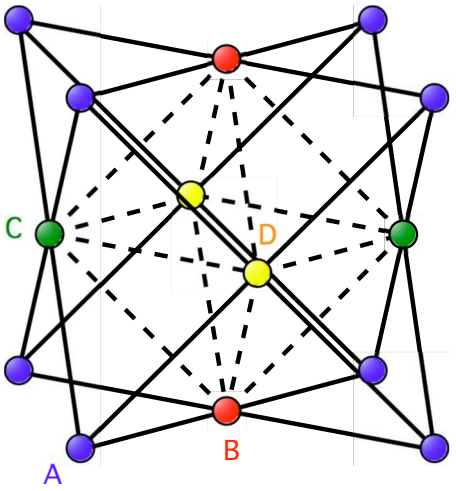

FIG. 18. (Color online) Conventional unit cell of the fcc lattice divided into four sublattices. The ansatz for the π-flux state corresponds to assigning hopping amplitude $+\chi$ to the bonds represented by solid lines and $-\chi$ to the bonds represented by the dashed lines.

$$\mathbf{r}^D_j = (1/2,0,1/2) + \mathbf{R}_j,$$

where $\mathbf{R}_j$ is a unit vector in the cubic lattice with lattice parameter $a=1$. We denote by F_{jA} the vector of spinon annihilation operators at site j of sublattice A and similarly for the other sublattices. We assign $\chi_{ij}=+\chi$ to the bonds connecting sites in sublattice A to all its nearest neighbors in sublattices B, C, D, and $\chi_{ij}=-\chi$ to the bonds connecting two sites that belong to sublattices B, C, or D. In other words, this ansatz corresponds to assigning $-\chi$ to the three bonds in the BCD base of each tetrahedron in the fcc lattice and $+\chi$ to the three bonds connecting the BCD base to the A vertex. As a result, there is π flux through every triangle and zero flux through every square in the fcc lattice. While this ansatz is clearly invariant under point-group transformations about A sites, it is also invariant under lattice translations, despite the fact that this permutes the four sublattices. This is because the corresponding changes in χ_{ij} can be removed by a gauge transformation. For instance, the gauge transformation

$$F_{jA} \to -F_{jA}, \quad F_{jB} \to -F_{jB},$$

$$F_{jC} \to F_{jC}, \quad F_{jD} \to F_{jD}, \tag{125}$$

exchanges the signs of χ_{ij} between sublattices A and B. It follows that the π-flux ansatz is invariant under point-group symmetries about any site of the fcc lattice and therefore respects all symmetries of the original Hamiltonian.

Minimizing the energy for the mean-field Hamiltonian with four sublattices, we find eight doubly degenerate bands for the π-flux state. Quarter filling is reached for dimensionless chemical potential $\mu\approx-1.68J$. The mean-field energy is

$$\frac{E_{\mathrm{MF}}}{\mathcal{N}\tilde{J}} = 2\chi\sum_{\lambda=1}^{8}\int\frac{d^3k}{(2\pi)^3}\theta[\mu-\tilde{\epsilon}_{\lambda}(\mathbf{k})]\tilde{\epsilon}_{\lambda}(\mathbf{k}) + 12\chi^2, \tag{126}$$

where the integral is over the reduced Brillouin zone of the cubic lattice. We find $E^{(\pi)}_{\mathrm{MF}}/\mathcal{N}=-0.053J$. This is lower than

the energy for the uniform state. We may also compare this to the *mean-field* energy of a VBS state (it is not so meaningful to compare these slave-particle mean-field energies directly to the variational energies quoted earlier for the Weiss mean-field and VBS states). For a mean-field VBS state, we take χ_{ij} nonzero only on a set of nonoverlapping dimers. In this case, we obtain $E_{\mathrm{VBS}}^{\mathrm{MF}}/\mathcal{N}=-1/18J\approx-0.055J$. This is slightly lower than the QSL states, but we expect that the energy of the spin-liquid states will be lowered by the Gutzwiller projection, since the latter is known to enhance spin-spin correlations.[43]

We note that both spin-liquid states have Fermi surfaces which are not nested and have no obvious instabilities. The states are also stable against bond anisotropy which enhances the hopping in a given plane. Perturbations to NN AFM exchange, such as next-nearest-neighbor interactions, will in general require more general ansatze for the bond matrix χ_{ij}. Nonetheless, as long as the perturbations are in some sense small, the χ_{ij} assumed in Eq. (109), in which hopping in a given plane occurs predominantly for two out of four spinon species, should be a good starting point for approximations.

VI. DISCUSSION

In this paper, we have introduced and analyzed a model to describe localized electrons in a $4d^1$ or $5d^1$ configuration on an fcc lattice, in which strong spin-orbit coupling and the t_{2g} orbital degeneracy combine to produce an effective $j=3/2$ description. The model contains three interactions—nearest-neighbor antiferromagnetic and ferromagnetic exchange, and electric quadrupolar interactions—and in addition may include the effect of structural anisotropy. We obtain the (Weiss) mean-field phase diagram, which includes three main phases, which all have a two-sublattice $\boldsymbol{Q}=2\pi(001)$ structure. In all the phases, large multipolar order parameters in addition to the usual magnetic dipolar order are present. Most remarkably, we find a broad regime of time-reversal invariant but quadrupolar ordered phase at intermediate temperatures. A spin-wave analysis indicates that quantum fluctuations are strong when nearest-neighbor antiferromagnetic exchange is dominant, and in this case, we suggest possible quantum-spin-liquid and valence-bond solid phases.

A. Experimental ramifications

The theory developed here can be applied and tested in a multitude of ways. Here we discuss a few of the main experimental properties which might be measured. First, there is the spatial symmetry breaking of the ordered phases. All the ordered states, at least in the cubic case, break lattice symmetries, and, in particular, double the unit cell. This can be tested in experiments such as neutron and x-ray scattering.

We discuss in some further detail the most intriguing case of the quadrupolar phase, which is nonmagnetic. It constitutes a type of real (time-reversal invariant) orbital ordering. It leads to a spontaneous splitting of the local quadruplet, breaking it down to an elemental Kramer's doublet. As such, this is not entirely distinct from a Jahn-Teller effect, in which ionic motions would lead to such splitting. In particular, even though in our model atomic displacements are not involved in an essential way, they would be expected at least to respond to the orbital order. In principle, this could be measured by scattering (x rays or neutrons) which accurately measure the crystal structure and symmetry. From the order parameter description of the quadrupolar phase, we can obtain the corresponding space group and crystal structure parameters to be sought in such a measurement. In particular, we find that the quadrupolar ordered phase corresponds to the tetragonal space group $P4_2/mnm$ (number 136). In this space group, apart from the doubling of the unit cell, one finds that all the A sites, B sites, and B' sites remain equivalent. However, the oxygen are no longer equivalent, but split into three classes, occupying the $4e$, $4f$, and $4g$ Wyckoff positions. Each of these positions has one degree of freedom which is not fixed by symmetry. Physically, the oxygen remains constrained to the simple cubic axes of the perovskite reference unit cell but may move by different amounts along each of the three axes. This is two more degrees of freedom than is found in the cubic $Fm\bar{3}m$ (number 225) space group, in which the oxygen maintain an ideal octahedron equidistant from each B (or B') site. While symmetry requires these structural changes, we do not have at present an estimate for their magnitude, which could be weak if coupling to the lattice is not strong.

Another quantity we have already discussed in Sec. IV E is the magnetic susceptibility, which shows signatures of the quadrupolar and ordering transitions. One complication is that the susceptibility is in many cases highly anisotropic and one may not be sure what component(s) are being measured in practice. Specifically, one may expect, if the system is ideal and fully in equilibrium, that the broken symmetry order parameters can be reoriented by the magnetic field, in such a way that they minimize the free energy. This will typically favor orientations which maximize the magnetic susceptibility. For instance, in the quadrupolar phase for cubic symmetry, this is an orientation with $\boldsymbol{Q}$ perpendicular to the field. However, such reorientation involves motion of domain walls and very large numbers of spins, and can easily be prevented by pinning or at least be incomplete in practice. Thus some diversity of behavior may be expected in experiment, as well as possibly hysteretic behavior even in the nonmagnetic state.

When the crystal is noncubic, one may explore the influence of single-ion anisotropy on the magnetic susceptibility. A naive application of Eq. (84) would immediately imply that single-ion terms do not contribute to the Curie-Weiss temperature as measured in the powder susceptibility. However, we caution that these equations hold only in the true high-temperature regime, in which $T\gg|D|$. If T is smaller than or comparable to $|D|$, higher-order terms in the high-temperature expansion are nontrivial, and a nonvanishing fitted Curie-Weiss temperature may result from D alone. Let us consider the powder susceptibility $\bar{\chi}$ for independent ions (i.e., neglecting exchange). One has

$$\bar{\chi}=\frac{\chi_{zz}}{3}+\frac{2\chi_{xx}}{3}=\frac{3}{4T}+\frac{\tanh D/T}{2D}, \tag{127}$$

in units of $g^2\mu_B^2$. We then suppose a linear fit to $1/\bar{\chi}$ versus T is made over a narrow region in the neighborhood of the

temperature $T_{\rm fit}$ and extrapolated to find the Curie-Weiss temperature as the intercept of the horizontal axis. The result is

$$\Theta_{\rm CW}(T_{\rm fit}) = -\frac{2T_{\rm fit}\left[T_{\rm fit}\sinh\left(\frac{2D}{T_{\rm fit}}\right)-2D\right]}{D\left[3\cosh\left(\frac{2D}{T_{\rm fit}}\right)+7\right]}. \quad (128)$$

Note that the fitted Curie-Weiss temperature is always negative, and is independent of the sign of D. It reaches a maximum in magnitude (at fixed D) of $\Theta_{\rm CW}\approx -0.18|D|$ when $T_{\rm fit}\approx 0.88|D|$, and only approaches zero very slowly when $T_{\rm fit}\gg|D|$: $\Theta_{\rm CW}\sim -\frac{4D^2}{15T_{\rm fit}}$. Conversely, at a fixed fitting temperature, the maximum achievable Curie-Weiss temperature is $\Theta_{\rm CW}\approx -0.26T_{\rm fit}$, when $|D|=1.84T_{\rm fit}$.

B. Materials survey

We now turn to a discussion of specific materials which have been studied experimentally.

1. Ba_2YMoO_6

We begin with the material Ba_2YMoO_6, which has been suggested experimentally to be an exotic "valence-bond glass" or to have a "collective spin-singlet" ground state. The expected separation between the $j=3/2$ and $j=1/2$ states in this material is over 2000 K so that the effective $j=3/2$ description used here should be excellent. Two recent experimental papers[12,13] observed an unusual behavior of the magnetic susceptibility, with *two* Curie regimes, such that $1/\chi$ is linear both above 100 K and below 50 K. Moreover, the magnetic specific heat shows a peak around 50 K, with Ref. 12 estimating the total magnetic entropy approximately equal to $R\ln 4$, as expected for $j=3/2$. Both these results suggest the existence of some single-ion anisotropy, which would explain the existence of two Curie regimes because it splits the fourfold degeneracy of the $j=3/2$ states but leaves a twofold Kramer's doublet at temperatures below $|D|$, which still gives a Curie signal. However, the cubic symmetry observed experimentally seems to rule out such an explanation. Moreover, the form of the powder susceptibility in Refs. 12 and 13 is qualitatively different from that expected for either fixed easy-plane or easy-axis anisotropy.

These difficulties are resolved if one considers the possibility of *spontaneous* anisotropy, which indeed is the primary characteristic of the quadrupolar ordered state. For example, the mean-field susceptibility for the cubic model with $J'=0.2J$, $V=0.3J$ is plotted in Fig. 13. At temperatures above the FM110 phase, one indeed observes two Curie regimes in the susceptibility, with a larger Curie constant at low temperature, as seen in the experiments. The kink in χ coincides with the quadrupolar ordering transition, and there is a peak in the specific heat at this temperature, also as observed in experiment. The theoretical specific heat has a second peak at lower temperatures, associated with magnetic ordering and exhaustion of the unsplit Kramer's doublet. We suggest that this peak is below the lowest temperatures measured, or perhaps is avoided due to disorder, and the spins falling out of equilibrium at low temperature. The fact that the Curie-Weiss temperature extracted *below* 50 K is only −2.3 K corroborates the notion that any magnetic ordering may be too low to observe or be obscured by the effects of disorder.

2. La_2LiMoO_6

La_2LiMoO_6 is monoclinic, the deviation from cubic symmetry arising primarily from rotations of the octahedra. The local coordination of the Mo sites is nearly perfectly octahedral with a weak tetragonal compression. The nature of crystal field effects, if significant, is unclear at present. Magnetically, the susceptibility shows, such as Ba_2YMoO_6, two apparent Curie regimes, separated by a kink at approximately 150 K. However, opposite to that material, La_2LiMoO_6 shows a smaller effective moment at low temperature compared to high temperature. In addition, the high-temperature Curie-Weiss temperature is $\Theta_{\rm CW}\approx -45$ K, significantly smaller than the kink temperature. Irreversibility distinguishing the behavior of the zero field coupling or field coupling susceptibility appears below 25 K.

The appearance of two Curie regimes again suggests either fixed or spontaneous magnetic anisotropy setting in around 150 K. However, the *reduction* in the effective moment below the kink in χ^{-1} is puzzling. We did not find this behavior in the powder susceptibility within our model with or without anisotropy modeled by D. As remarked above, however, the actual nature of the crystal-field anisotropy in La_2LiMoO_6 is unclear. If it is significant and different in form from the D term, this might explain the behavior. Single-crystal studies would be helpful in elucidating the situation.

3. Sr_2CaReO_6 *and* Sr_2MgReO_6

Sr_2CaReO_6 and Sr_2MgReO_6 have distorted perovskite structures, with monoclinic and tetragonal symmetry, respectively.[14,15] Experimentally, the materials are notable for their very high antiferromagnetic Curie-Weiss temperature, $-\Theta_{\rm CW}\gtrsim 400$ K. Susceptibility and specific-heat measurements show anomalies suggestive of freezing and/or short-range ordering at 14 K and 50 K, for Sr_2CaReO_6 and Sr_2MgReO_6, respectively. Two possible interpretations of this behavior are: (1) the Curie-Weiss temperature is dominated by strong exchange but fluctuations largely suppress ordering, or (2) the Curie-Weiss temperature is due largely to single-ion effects, and the true exchange scale is comparable to the observed anomalies in χ and c_v.

In the former scenario, the key question is why these two materials show so much larger exchange than do the other compounds in this family. From the point of view of this work, attributing the Curie-Weiss temperature to exchange alone would imply J is actually comparable to the SOC, so that the projection to $j=3/2$ may even be suspect. The Curie-Weiss temperatures are sufficiently large that one may suspect that the $5d$ electrons are not so well localized and the system is close to a Mott transition. It would be interesting to measure their optical properties to address this possibility.

The latter explanation seems possible, as both materials show significant deviations from the cubic structure:

Sr_2CaReO_6 is monoclinic while Sr_2MgReO_6 is tetragonal. The actual distortions of the octahedra are rather small in both cases, the *Re*-O distance varying by only about 0.02 Å at room temperature. However, there are significant rotations and tilts of the octahedra, and crystal-field splittings of the $j=3/2$ quadruplet are certainly allowed. Examination of the *Re*-O bond lengths suggests easy-axis anisotropy. From Eq. (128), we see that, in principle, a negative Curie-Weiss temperature could be attributed to D. However, from the present model we cannot obtain such a large value, which in these two materials is comparable or larger than the fitting temperature. Nevertheless, we may imagine that some combination of exchange and single-ion anisotropy may conspire to produce the observed behavior.

If we assume a large easy-axis anisotropy, we would then expect, based on the analysis in Sec. III A 1, to have an AFM ground state. The anomalies might be related to this ordering. Experimentally, spin freezing and irreversibility is observed but without clear signs of long-range ordering. The experimentalists caution that, due to the small magnetic moment of the Re^{6+} ions, a small ordered component could not be ruled out in either material.[14,15] Indeed, in the AFM state, a very small moment is expected, due to the primacy of octupolar order.

While this is promising, we note that it is likely that several effects not in our model play a role. First, the structure of the materials is not a simple compression of the cubic structure and so the crystal fields might have a significantly different form from the simple D term. This is especially true in Sr_2CaReO_6, which has the more distorted monoclinic structure. Second, in Sr_2MgReO_6, the *Re*-O-Mg bond angles are very different in the XY plane (160°) and normal to it (180°),[14] so substantial spatial anisotropy in the exchange couplings may be present. This is not included in our model. Also in Sr_2MgReO_6, the ZFC and FC susceptibility actually diverge already around 300 K, which suggests a high degree of disorder in this material, which might be responsible for converting the AFM to a glassy state.

One indication supporting an antiferromagnetic ground state is the observation, in Sr_2CaReO_6, of a T^3 magnetic contribution to the specific heat, in contrast to the usual linear one characteristic of a spin glass. The T^3 behavior would naturally be expected from spin waves in the AFM state, which as we have noted displays gapless spin waves, at least in the semiclassical approximation. Such T^3 behavior might even persist if the AFM order had a finite correlation length, due to Halperin-Saslow modes,[44] as recently postulated in $NiGa_2S_4$.[45] A T-linear specific heat was observed in Sr_2MgReO_6, albeit with a small coefficient.[14] As we have already remarked, however, this material is likely to be more disordered, consistent with the more conventional spin-glasslike specific heat.

While these considerations seem reasonable, they are hardly definitive. Further studies, particularly on single crystals, would be most helpful in clarifying the physics of these materials.

4. Ba_2CaReO_6

In Ba_2CaReO_6, there is a structural transition from a high-temperature cubic phase to a low-temperature tetragonal one, with a doubled unit cell, at $T=120$ K.[16] The experimentalists have fitted the low-temperature structure to the $I4/m$ space group. From this fit, they found an elongation along the c (or z) axis but a slight compression of the ReO_6 octahedra. One may consider two possibilities. Either this is indeed the correct symmetry, in which case it must have structural origin not related to the 5*d* electrons, *or* this transition in fact coincides with the quadrupolar ordering described here, which also gives a tetragonal state with the same unit cell. The $P4_2/mnm$ space group was not considered in Ref. 16.

A small, negative Curie-Weiss temperature $\Theta_{CW}=-39$ K was measured by fitting the susceptibility in the high-temperature cubic phase, indicating that J' should be not too large. A predominantly antiferromagnetic ordering transition was observed at $T=15$ K, which is consistent with our expectations in the small J' and V regime (recall that an antiferromagnetic state is expected both with and without single-ion anisotropy in this parameter range). It would be interesting to compare the predicted magnetic structure in the AFM or AFM′ phase with experiment, by carrying out neutron-scattering and NMR measurements.

5. Ba_2NaOsO_6

Ba_2NaOsO_6,[18] is one of only two examples in this class in which single-crystal experiments have been performed, to our knowledge. A transition at $T=6.8$ K was found to a ferromagnetic state with easy axis along a [110] direction. Within the experimental resolution, the material was found to remain cubic down to the lowest measured temperature. A fit to Curie-Weiss behavior found a negative Curie-Weiss temperature, $-13<\Theta_{CW}<-10$ K, depending upon field orientation. We note that this is compatible with Eq. (84), and suggests that the material is in the regime of larger V and smaller J'. In this region, we expect a high-temperature quadrupolar transition, well above the ferromagnetic state. While no such transition is observed in the experiment, the magnetic specific heat of such a transition may be masked by the lattice contribution at higher temperature, and the signature in susceptibility may be subtle.

Several other indications are in favor of this scenario. First, the susceptibility continues to display pronounced anisotropy, favoring the [110] direction, up to at least 200 K, well above the ferromagnetic transition. This would indeed be expected in the quadrupolar ordered state. Second, the magnetic specific heat divided by temperature, integrated over the peak up to about 15 K gives a magnetic entropy of approximately $R\ln 2$, which is only half the expected entropy for the $j=3/2$ quadruplet. This entropy may be released over a significantly higher temperature range, up to the quadrupolar ordering transition. Third, the observation itself of ferromagnetism with a [110] easy axis is a marked success of our theory. This type of anisotropy is not natural from the standpoint of Landau theory, within which cubic anisotropy manifests itself at leading order as a term in the free energy of the form $v[(M^x)^4+(M^y)^4+(M^z)^4]$ ($\boldsymbol{M}$ is the magnetization), which, depending upon the sign of v, generates a [111] or [100] easy axis. A continuous Landau transition to the FM110 state is instead made possible by the fact

that the quadrupolar order already breaks the cubic symmetry in the paramagnetic state.

It would be interesting to further probe the system to establish in more detail the correspondence (or lack thereof) with our theoretical predictions. The predicted tetragonal distortion of the cubic structure would be a natural quantity to seek in experiment. This also manifests locally in the magnetism, since although the net magnetization is aligned with the [110] axis, the local spin expectation values are not. This might be measurable for instance by a local probe such as NMR.

We note that the first-principles calculation in Ref. 46 also points that the spin-orbit interaction is responsible for the small magnetic moment observed in Ba_2NaOsO_6. This result is consistent with our prediction. The authors attribute the lack of structural distortion in the low-temperature ferromagnetic phase to a cooperative effect of electron correlation and SOC. Our predictions on the lattice distortion are based on a symmetry analysis of the finite-temperature quadrupolar ordered phase. It would also be interesting to explore the finite-temperature structure properties by first-principles methods.

6. Ba_2LiOsO_6

Ba_2LiOsO_6 has also been grown in single-crystal form. The structure was determined to be cubic by x-ray diffraction at room temperature.[17] Aside from this diffraction data, only bulk magnetic susceptibility results are available. One observes a negative Curie-Weiss temperature $\Theta_{CW} \approx -40$ K, and an apparent antiferromagnetic transition at $T_N \approx 8$ K. This appears largely consistent with the expected behavior in region I of Fig. 6.

C. Comparison and future work

We are aware of only one other theoretical work studying this class of materials. Lee and Pickett[38] performed electronic-structure calculations for Ba_2NaOsO_6 and Ba_2LiOsO_6, emphasizing the role of SOC. We completely agree with the conclusion that SOC plays a crucial role in the magnetism. However, the magnetic structure and phase transitions were not addressed.

Our study is much more comprehensive, and gives a great deal of guidance both for future theory and experiment. Many experimental suggestions have already been made. In particular, verification of the quadrupolar ordering transition would be especially exciting. On the theoretical side, the problem of the effects of quantum fluctuations in the small J' and V limit remains rather open. It would be remarkable if a spin-liquid or valence-bond solid state could be established for this highly non-SU(2) symmetric and nominally "large" spin $j=3/2$ model. To do so would require some hard theoretical work applying more quantitative numerical methods to our model Hamiltonian. A natural extension of this work would be to consider the "higher spin" analogs of these materials, with $4d^2$ or $5d^2$ electronic states. As there is still partial occupation of the t_{2g} orbitals in this case, we expect SOC again to play a dominant role, and interesting multipolar physics is likely present.

ACKNOWLEDGMENTS

We thank John Greedan, Ian Fisher, and Ram Seshadri for useful discussions. This work was supported by the DOE through Basic Energy Sciences Grant No. DE-FG02-08ER46524. L.B.'s research facilities at the KITP were supported by the National Science Foundation under Grant No. NSF PHY-0551164.

[1] T. Moriya, Phys. Rev. **120**, 91 (1960).
[2] I. Dzyaloshinsky, J. Phys. Chem. Solids **4**, 241 (1958).
[3] G. Chen and L. Balents, Phys. Rev. B **78**, 094403 (2008).
[4] G. Jackeli and G. Khaliullin, Phys. Rev. Lett. **102**, 017205 (2009).
[5] N. Büttgen, J. Hemberger, V. Fritsch, A. Krimmel, M. Mücksch, H.-A. K. von Nidda, P. Lunkenheimer, R. Fichtl, V. Tsurkan, and A. Loidl, New J. Phys. **6**, 191 (2004).
[6] V. Fritsch, J. Hemberger, N. Büttgen, E.-W. Scheidt, H.-A. Krug von Nidda, A. Loidl, and V. Tsurkan, Phys. Rev. Lett. **92**, 116401 (2004).
[7] A. Krimmel, M. Mücksch, V. Tsurkan, M. M. Koza, H. Mutka, and A. Loidl, Phys. Rev. Lett. **94**, 237402 (2005).
[8] G. Chen, L. Balents, and A. P. Schnyder, Phys. Rev. Lett. **102**, 096406 (2009).
[9] G. Chen, A. P. Schnyder, and L. Balents, Phys. Rev. B **80**, 224409 (2009).
[10] S. Sarkar, T. Maitra, R. Valentí, and T. Saha-Dasgupta, Phys. Rev. B **82**, 041105 (2010).
[11] E. J. Cussen, D. R. Lynham, and J. Rogers, Chem. Mater. **18**, 2855 (2006).
[12] M. A. de Vries, A. C. Mclaughlin, and J.-W. G. Bos, Phys. Rev. Lett. **104**, 177202 (2010).
[13] T. Aharen, J. E. Greedan, C. A. Bridges, A. A. Aczel, J. Rodriguez, G. MacDougall, G. M. Luke, T. Imai, V. K. Michaelis, S. Kroeker, H. Zhou, C. R. Wiebe, and L. M. D. Cranswick, Phys. Rev. B **81**, 224409 (2010).
[14] C. R. Wiebe, J. E. Greedan, P. P. Kyriakou, G. M. Luke, J. S. Gardner, A. Fukaya, I. M. Gat-Malureanu, P. L. Russo, A. T. Savici, and Y. J. Uemura, Phys. Rev. B **68**, 134410 (2003).
[15] C. R. Wiebe, J. E. Greedan, G. M. Luke, and J. S. Gardner, Phys. Rev. B **65**, 144413 (2002).
[16] K. Yamamura, M. Wakeshima, and Y. Hinatsu, J. Solid State Chem. **179**, 605 (2006).
[17] K. E. Stitzer, M. D. Smith, and H.-C. zur Loye, Solid State Sci. **4**, 311 (2002).
[18] A. S. Erickson, S. Misra, G. J. Miller, R. R. Gupta, Z. Schlesinger, W. A. Harrison, J. M. Kim, and I. R. Fisher, Phys. Rev. Lett. **99**, 016404 (2007).
[19] P. Santini, S. Carretta, G. Amoretti, R. Caciuffo, N. Magnani, and G. H. Lander, Rev. Mod. Phys. **81**, 807 (2009).
[20] K. Haule and G. Kotliar, Nat. Phys. **5**, 796 (2009).
[21] G. Jackeli and G. Khaliullin, Phys. Rev. Lett. **103**, 067205 (2009).

[22] E. M. Stoudenmire, S. Trebst, and L. Balents, Phys. Rev. B **79**, 214436 (2009).
[23] A. Läuchli, F. Mila, and K. Penc, Phys. Rev. Lett. **97**, 087205 (2006).
[24] H. Tsunetsugu and M. Arikawa, J. Phys. Soc. Jpn. **75**, 083701 (2006).
[25] S. Bhattacharjee, V. B. Shenoy, and T. Senthil, Phys. Rev. B **74**, 092406 (2006).
[26] S. Nakatsuji, Y. Nambu, H. Tonomura, O. Sakai, S. Jonas, C. Broholm, H. Tsunetsugu, Y. Qiu, and Y. Maeno, Science **309**, 1697 (2005).
[27] L. Balents, Nature (London) **464**, 199 (2010).
[28] P. Anderson, Mater. Res. Bull. **8**, 153 (1973).
[29] X.-G. Wen, Phys. Rev. B **65**, 165113 (2002).
[30] O. I. Motrunich, Phys. Rev. B **73**, 155115 (2006).
[31] S. Ryu, O. I. Motrunich, J. Alicea, and M. P. A. Fisher, Phys. Rev. B **75**, 184406 (2007).
[32] Y. Okamoto, M. Nohara, H. Aruga-Katori, and H. Takagi, Phys. Rev. Lett. **99**, 137207 (2007).
[33] M. J. Lawler, A. Paramekanti, Y. B. Kim, and L. Balents, Phys. Rev. Lett. **101**, 197202 (2008).
[34] M. Hermele, M. P. A. Fisher, and L. Balents, Phys. Rev. B **69**, 064404 (2004).
[35] J. Chaloupka, G. Jackeli, and G. Khaliullin, Phys. Rev. Lett. **105**, 027204 (2010).
[36] C. L. Henley, J. Appl. Phys. **61**, 3962 (1987).
[37] S. Murakami, N. Nagaosa, and S.-C. Zhang, Phys. Rev. B **69**, 235206 (2004).
[38] K.-W. Lee and W. Pickett, EPL **80**, 37008 (2007).
[39] R. Shiina, O. Sakai, H. Shiba, and P. Thalmeier, J. Phys. Soc. Jpn. **67**, 941 (1998).
[40] Y. Q. Li, M. Ma, D. N. Shi, and F. C. Zhang, Phys. Rev. Lett. **81**, 3527 (1998).
[41] A. Joshi, M. Ma, F. Mila, D. N. Shi, and F. C. Zhang, Phys. Rev. B **60**, 6584 (1999).
[42] A. Del Maestro and M. J. P. Gingras, Phys. Rev. B **76**, 064418 (2007).
[43] F. C. Zhang, C. Gros, T. M. Rice, and H. Shiba, Supercond. Sci. Technol. **1**, 36 (1988).
[44] B. I. Halperin and W. M. Saslow, Phys. Rev. B **16**, 2154 (1977).
[45] D. Podolsky and Y. B. Kim, Phys. Rev. B **79**, 140402 (2009).
[46] H. J. Xiang and M.-H. Whangbo, Phys. Rev. B **75**, 052407 (2007).